



University of Kentucky
UKnowledge

University of Kentucky Master's Theses

Graduate School

2004

SCALE MODEL EXPERIMENTS AND NUMERICAL STUDY ON A STEEL TEEMING PROCESS

Pavan Kumar Singh
University of Kentucky

[Right click to open a feedback form in a new tab to let us know how this document benefits you.](#)

Recommended Citation

Singh, Pavan Kumar, "SCALE MODEL EXPERIMENTS AND NUMERICAL STUDY ON A STEEL TEEMING PROCESS" (2004). *University of Kentucky Master's Theses*. 317.
https://uknowledge.uky.edu/gradschool_theses/317

This Thesis is brought to you for free and open access by the Graduate School at UKnowledge. It has been accepted for inclusion in University of Kentucky Master's Theses by an authorized administrator of UKnowledge. For more information, please contact UKnowledge@lsv.uky.edu.

ABSTRACT OF THESIS

SCALE MODEL EXPERIMENTS AND NUMERICAL STUDY ON A STEEL TEEMING PROCESS

During the teeming process of molten steel from a ladle, a bathtub-type vortex may be formed in the ladle. The vortex entrains undesired slag on the surface into the tundish, lowering the quality. The formation of such vortices has been studied using two different scale models. Since the kinematic viscosity of water is similar to that of molten steel, the molten steel was simulated by water in the experiments. The Particle Image Velocimetry (PIV) technique was used to measure water flow patterns. Results show that the initial tangential velocity of water is responsible for the vortex formation. The effects of Reynolds and Froude numbers on the vortex formation were investigated and Froude number was found to be the dominant pi-number. A Computational Fluid Dynamics (CFD) modeling was also conducted to simulate the vortex formation with good agreement with the experiments.

Keywords: Teeming, Ladle, Vortex, Scale models, PIV, Initial Tangential Velocity, Reynolds number, Froude number.

Pavan Kumar Singh

Date: 03/12/04

**SCALE MODEL EXPERIMENTS AND NUMERICAL STUDY
ON A STEEL TEEMING PROCESS**

By

Pavan Kumar Singh

Dr. Kozo Saito
Director of Thesis

Dr. George Huang
Director of Graduate Studies

Date: 03/12/2004

RULES FOR THE USE OF THESIS

Unpublished thesis submitted for the Master's degree and deposited in the University of Kentucky Library are as a rule open for inspection, but are to be used only with due regard to the rights of the authors. Bibliographical references may be noted, but quotations or summaries of parts may be published only with the permission of the author, and with the usual scholarly acknowledgements.

Extensive copying or publication of the thesis in whole or in part also requires the consent of the Dean of the Graduate School of the University of Kentucky.

THESIS

Pavan Kumar Singh

The Graduate School
University of Kentucky
2004

**SCALE MODEL EXPERIMENTS AND NUMERICAL STUDY
ON A STEEL TEEMING PROCESS**

THESIS

A thesis submitted in partial fulfillment of the requirements
for the degree of Master of Science in the
College of Engineering at the
University of Kentucky

By

Pavan Kumar Singh

Lexington, Kentucky

Director: Dr. Kozo Saito

(Professor of Mechanical Engineering)

Lexington, Kentucky

2004

..... **To My Parents**

ACKNOWLEDGMENTS

It is a pleasure to express a deep sense of gratitude and appreciation to my advisor and thesis Chairman, Professor Kozo Saito for his supervision and assistance throughout the course of this study. I have been extremely humbled by his intellect and motivated by his encouragement and I am thankful that he was a major influence in my masters' experience. I wish to acknowledge and appreciate the support of Dr. Kazunori Kuwana and Dr. Mohamed Hassan for their assistance in Numerical study and Experimental work respectively. This work would not have been complete without their patience and instructive comments and evaluation at every stage.

Further, I wish to thank the other members on my thesis evaluation committee: Dr. Larry Holloway and Dr. Keith Rouch for their valuable insights and feedbacks that challenged my thinking to improve substantially the final form of this thesis. This study was sponsored by Nippon Steel Corporation, Japan. I am grateful to Mr. Junichi Nakagawa (Nippon Steel Corporation) and Mr. Kozo Sekimoto (Sekimoto SE Engineering, Japan) for valuable technical discussions.

Thanks are also due to the members of the machine shop of the Manufacturing Centre at the University of Kentucky for fabricating various components of the experimental apparatus. I am also thankful to all my colleagues in the Industrial Applications and Engineering Science (IAES) research group for their vital support throughout. Lastly, but most importantly, I would like to express my gratitude to my parents, to whom this work is dedicated, and siblings, for all the encouragement and support.

TABLE OF CONTENTS

ACKNOWLEDGMENTS	iii
LIST OF FIGURES	vi
LIST OF FILES.....	viii
CHAPTER 1	1
1.1 INTRODUCTION.....	1
1.2 NOMENCLATURE	1
1.3 CHARACTERISTICS OF VORTEX FUNNELS.....	1
1.3.1 <i>Vortexing Funnel</i>	2
1.3.2 <i>Stages in the Formation of a Vortexing Funnel</i>	3
1.3.3 <i>Direction of Rotation of Vortexing Funnel</i>	3
1.3.4 <i>Characteristic Features of a Vortexing Funnel</i>	4
1.4 THE CONTINUOUS CASTING PROCESS.....	4
1.4.1 <i>Two types of gravity-driven drainage</i>	5
1.4.2 <i>Geometry and dimensions of continuous casting vessels</i>	5
1.4.3 <i>Tangential velocity distributions in various vessels</i>	6
1.5 IMPLICATIONS OF SLAG ENTRAINMENT.....	7
1.5.1 <i>Metal Cleanness</i>	7
1.5.2 <i>Productivity</i>	8
1.5.3 <i>Yield of Liquid Steel</i>	8
1.5.4 <i>The End of Drainage Decision</i>	8
1.6 OBJECTIVES OF THE PRESENT WORK	8
1.7 STRUCTURE OF THE REMAINDER OF THE THESIS.....	9
CHAPTER 2	10
2.1 CURRENT UNDERSTANDING OF SLAG ENTRAINING FUNNEL FORMATION	10
2.2 THEORETICAL BACKGROUND.....	12
2.2.1 <i>Vorticity and Circulation</i>	12
2.3 HYDRODYNAMIC PRINCIPLES OF VORTEX FORMATION	14
2.3.1 <i>Principle of Conservation of Angular Momentum</i>	14
2.4 FREE AND FORCED VORTICES	15
2.4.1 <i>Free Vortex</i>	15
2.4.2 <i>Forced Vortex</i>	16
2.5 <i>Vortex plus Sink-logarithmic spiral surface flow lines</i>	16
2.6 THE SURFACE PROFILE OF THE POTENTIAL VORTEX	18
2.7 RANKINE COMBINED VORTEX.....	19
CHAPTER 3	21
3.1 EXPERIMENTAL SETUP.....	21
3.2 PRELIMINARY OBSERVATIONS	22
3.3 EXPERIMENTS USING PARTICLE IMAGE VELOCITOMETRY	23
3.3.1 <i>Principle of PIV</i>	23
CHAPTER 4	27
4.1 INTRODUCTION.....	27
4.1.1 <i>The Volume Fraction Equation</i>	27
4.1.2 <i>The Momentum Equation</i>	28
4.2 RESULTS OF NUMERICAL SIMULATION	28
4.2.1 <i>Temporal Behavior of water surface</i>	28

4.2.2 Velocity Flow fields	28
CHAPTER 5	31
4.1 INTRODUCTION	31
4.2 SCALING LAWS FORMULATION	31
CHAPTER 6	34
6.1 INTRODUCTION	34
6.2 CHARACTERISTICS OF TANGENTIAL VELOCITY	34
6.3 VARIATION OF CRITICAL HEIGHTS WITH VARYING INITIAL TANGENTIAL VELOCITIES	35
6.4 NON-DIMENSIONAL PLOTS OF INITIAL TANGENTIAL VELOCITY VS. CRITICAL HEIGHT	38
6.4.1 Variation of Non-Dimensional Critical Height (H_{cr}/H_j) with Reynolds Number (Re).....	39
6.4.2 Variation of Non-Dimensional Critical Height (H_{cr}/H_j) with Froude Number (Fr).....	42
6.5 RELATIVE SIGNIFICANCE OF GOVERNING FORCES	45
6.6 RELATION BETWEEN FROUDE NUMBER AND NON-DIMENSIONAL CRITICAL HEIGHT	45
6.7 RESULTS FOR EXPERIMENTS USING PIV WITH VERTICAL LASER BEAM	45
CHAPTER 7	48
7.1 INTRODUCTION	48
7.2 CONCLUDING REMARKS	48
7.3 MODELING OF VORTEXING FUNNEL FORMATION	49
7.4 FUTURE WORK	49
APPENDIX	50
NOMENCLATURE	50
REFERENCES.....	52
VITA.....	54

LIST OF FIGURES

Figure 1.1: Stages in the development of a vortexing funnel	4
Figure 1.2: Continuous Casting Process	5
Figure 2.1: Vorticity and Circulation.....	13
Figure 2.2: Graphical representation of a line vortex and a line sink.....	17
Figure 2.3: Streamlines for a vortex plus sink constructed by a graphical method	18
Figure 2.4: Rankine combined vortex	20
Figure 3.1: Schematic of scale models and photograph.....	21
Figure 3.2: Experimental setup.....	22
Figure 3.3: Surface profile observed using food color (in the presence of vortex).....	23
Figure 3.4: Image capturing using Digital camera and PIV	24
Figure 3.5: Experimental setup with PIV (horizontal laser beam)	25
Figure 3.6: Experimental setup with PIV (vertical laser beam)	25
Figure 4.1: History of water surface location ($\Omega = 0.5$ 1/s)	29
Figure 4.2: History of water surface location ($\Omega = 1.5$ 1/s)	29
Figure 4.3: Predicted velocity fields ($\Omega = 1.5$ 1/s).....	30
Figure 6.1: Variation of tangential velocity along the radius.....	35
Figure 6.2: Critical height vs. initial tangential velocity (big model)	36
Figure 6.3: Critical height vs. initial tangential velocity (small model)	37
Figure 6.4: Comparison of experimental and numerical results	37
Figure 6.5: Non-Dimensional Critical Height vs. Reynolds Number (big model).....	39
Figure 6.6: Non-Dimensional Critical Height vs. Reynolds Number (small model)	40
Figure 6.7: Comparison of non-Dimensional Critical Height vs. Reynolds Number.....	41
Figure 6.8: Comparison of experimental and numerical results	41
Figure 6.9: Non-Dimensional Critical Height vs. Froude Number (big model)	43

Figure 6.10: Non-Dimensional Critical Height vs. Froude Number (small model)	43
Figure 6.11: Comparison of non-Dimensional Critical Height vs. Froude Number	44
Figure 6.12: Comparison of experimental and numerical results	44
Figure 6.13: Curve fitting for the H_{cr} / H_i vs. Fr plot	46
Figure 6.14: Top view PIV image and velocity profiles (no vortex)	47
Figure 6.15: Side view of velocity profile (with vortex)	47

LIST OF FILES

<i>File</i>	<i>Type</i>	<i>Size</i>
<i>PKthesis</i>	<i>pdf</i>	<i>1.06 MB</i>

CHAPTER 1

INTRODUCTION

1.1 INTRODUCTION

The minimization of slag entrainment has been a major concern in steelmaking processes for a long time. In particular, slag entrainment caused by the formation of what is commonly known as a vortex has been a reason for much concern of every quality-conscious steelmaker today. This thesis is aimed to address, and improve the understanding and control of this malicious affect of the vortex induced slags towards the overall efficiency of steelmaking process. The goal of this first chapter is to define, state the objectives, and chart a structure for the rest of this thesis. The phenomenon of slag entraining funnel formation will be introduced, along with its impact on the continuous casting process.

1.2 NOMENCLATURE

This thesis is concerned with the premature entrainment of supernatant slag layer during the drainage of the various metallurgical vessels used in the continuous casting of steel. Such slag entrainment is known to occur well before the vessel is empty of liquid steel, and leads to metal cleanness problems. Thus it is a normal steelmaking practice to stop emptying the vessel before any slag entrainment can begin, even though this means a loss in yield of liquid steel. Thus, the prevention of premature slag entrainment will not only improve steel cleanness, but will also improve the yield of liquid steel by permitting more complete emptying of the vessel. An additional reason to prevent slag entrainment is that measures necessary to recover from the adverse effects of slag entrainment usually result in a serious loss of productivity and an increase in production costs.

Such premature slag entrainment is commonly attributed to what is known as the “vortex,” as in air-entraining, funnel shaped vortex that occurs in bath-tubs, wash-basins and kitchen-sinks. The subject of vortex formation has fascinated scientists and engineers alike for so long that it is not surprising that literally hundreds and hundreds of technical papers have been published on the subject. An essential pre-requisite to the formation of such a vortex is that the liquid being drained, or emptied, out of a holding vessel possesses some rotational motion, whatever the source of such rotation.

1.3 CHARACTERISTICS OF VORTEX FUNNELS

Before discussing the ramifications of slag entrainment on metal cleanness, the yield of liquid steel, and productivity of the continuous casting process, it is necessary to briefly describe some of the well known features of vortexing funnels.

1.3.1 Vortexing Funnels

As mentioned earlier, the presence of rotational motion is necessary for the formation of a vortexing funnel during the drainage of a holding vessel. Vortexing funnels are known to occur in holding vessels of various shapes and sizes. A holding vessel, by definition, has an inflow and an outflow and a means to hold the liquid, if necessary. Two types of holding vessel drainage modes are known, *viz.* (1) steady-state, *constant-head drainage* and (2) nonsteady-state, *batch-type drainage*. During *constant-head drainage*, the liquid head in the holding vessel is maintained constant, the flow rates of liquid entering and leaving the vessel being roughly equal at all times. During batch-type drainage, there is usually no inflow into the vessel during the drainage itself, and the liquid head continues to decrease as the drainage progresses. The outflow nozzle may be a drainage nozzle at the bottom or side wall, or it may be a vertical intake pipe through which liquid is pumped upwards and out.

From the point of view of avoiding the entrainment of any supernatant fluid during the drainage of a holding vessel, the most important property of vortexing funnel formation is the critical liquid head, $H_{cr,v}$, for its formation. A second property that has been of considerable interest to various authors is the discharge coefficient, C_d , of drainage nozzles in the presence of an air-entraining vortexing funnel. The stronger the rotational motion in the vessel, the larger is the size of the funnel formed; the larger the vortexing funnel, the greater is the volume of air entrained; the lower is the flow rate of liquid flowing through the drainage orifice. Thus, defining C_d as the ratio of the actual liquid flow rate to the theoretical flow rate (for an identical liquid head) where the drainage nozzle or orifice was flowing full of liquid, it can be stated that vortexing funnel formation is always accompanied by a decrease in the coefficient of discharge, C_d , of the drainage nozzle or orifice.

It is interesting to note that the $H_{cr,v}$ was rarely a parameter of interest in studies that were concerned mainly with C_d , a possible implication that a vortexing funnel could be formed from any desired liquid head, provided sufficiently strong rotational forces were present. Likewise, studies aimed at understanding $H_{cr,v}$ rarely attempted to analyze C_d , the implication here being that the events that followed vortexing funnel formation were largely irrelevant to the process

under consideration-- after all, the process would be best served if the vortexing funnel formation, and the associated entrainment of supernatant fluid, was suppressed altogether. Thus, the understanding of C_d is only of academic interest to steelmakers and shall not be considered in the present study.

1.3.2 Stages in the Formation of a Vortexing Funnel

There is general consensus among researchers that a vortexing funnel goes through four stages of development as sketched in Figure 1.1. In the first stage, where the liquid head is very large and/or any residual tangential velocity is low, a tiny dimple is formed on the surface, usually centered on the axis of rotation of the tangential motion. Then as the liquid head decreases, or as the residual tangential velocity increases, the dimple starts extending down a deeper vortex funnel whose tip shows rapid rotation, and finally a fully developed vortexing funnel that entrains the supernatant air into the nozzle.

The rate of progress through the four stages itself is dependent on the residual tangential velocity, and its spatial distribution in the holding vessel. In the presence of strong tangential velocities, progress from the dimple to the fully developed vortexing funnel is almost instantaneous. When the residual tangential velocities are weaker, the dimple would take longer to grow into a fully developed vortexing funnel, and the diameter of the funnel would be much smaller as well.

After becoming a fully developed vortexing funnel, further decrease in the liquid head is usually accompanied by an increase in the diameter of the vortexing funnel, and consequently, an increase in the amount of supernatant air entrained.

It must be noted that the sketches in Figure 1.1 are simplifications of reality. Vortexing funnels are rarely as symmetrical as sketched, except in the case of very weak residual tangential velocities. In the presence of stronger tangential velocities, a helical spiral-like surface is superimposed on the funnel shape; the funnel also moves laterally and spatially with time.

1.3.3 Direction of Rotation of Vortexing Funnel

The direction of rotation of any vortexing funnel is always the same as the direction of any residual tangential motion in the vessel. This can be easily verified by alternately inducing clockwise and counterclockwise rotational motions in any given holding vessel, and observing the vortexing funnel motion.

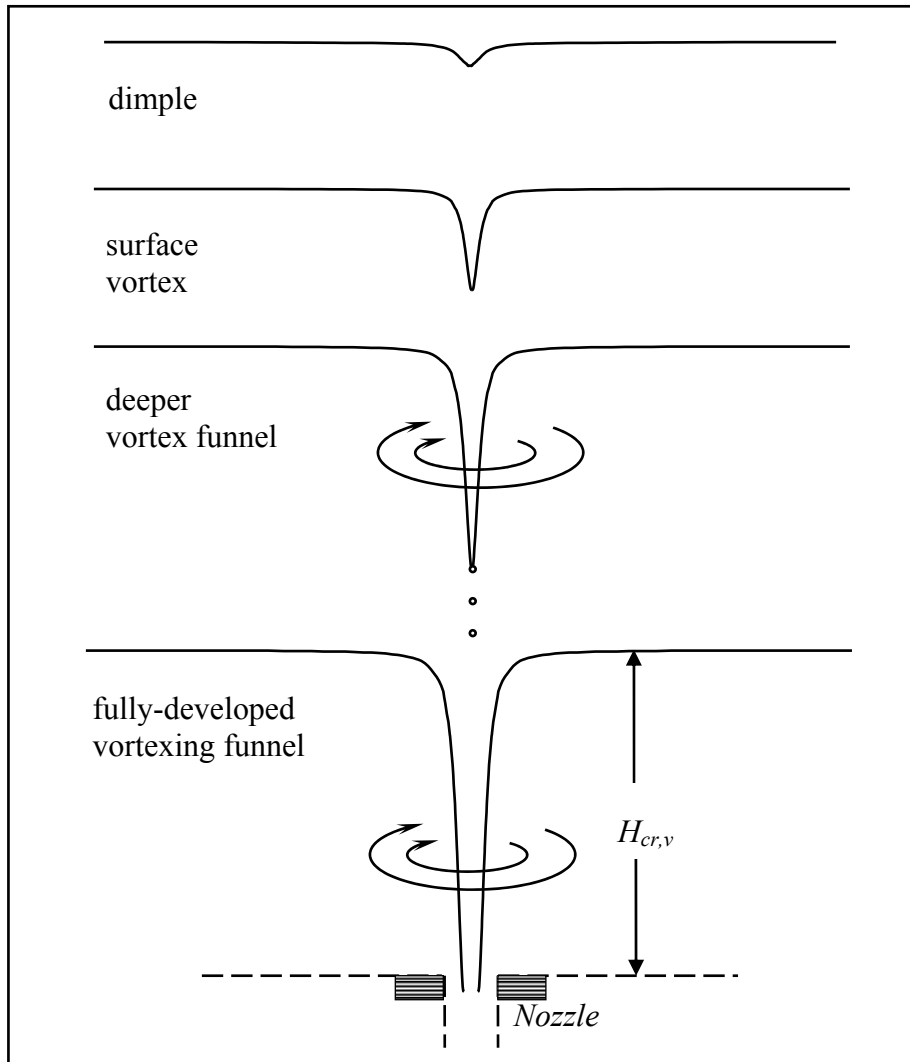


Figure 1.1: Stages in the development of a vortexing funnel

In the case of industrial holding vessels, the residual tangential velocity distribution will be a function of the inflow conditions, temperature gradients, external stirring actions that are part of the process.

1.3.4 Characteristic Features of a Vortexing Funnel

The characteristics of a vortexing funnel formed in a holding vessel drained through the bottom are

- (a) $H_{cr,v}$, the critical liquid height at which the vortexing funnel becomes fully developed i.e. reaches the bottom of the vessel.
- (b) The minimum residual tangential velocity, $V_{\theta,cr}$, necessary for the initiation of a vortex.

1.4 THE CONTINUOUS CASTING PROCESS

Tonnage steel is now produced primarily through the continuous casting process. While proceeding from the steelmaking furnace to the final cast product (variously called as slab, bloom or billet, depending upon its dimensions), the liquid steel passes through four different metallurgical vessels. The first vessel is the furnace, which would be a BOF (Basic Oxidising Furnace) converter in most integrated steel mills, or an EAF (Electric Arc Furnace) in most mini-steel mills. The furnace is “tapped” into the ladle, where it may or may not undergo further secondary metallurgical reactions. The ladle of steel is then “teemed” (emptied) into the tundish, from which it is “poured” or distributed to a set of moulds of the continuous casting machine.

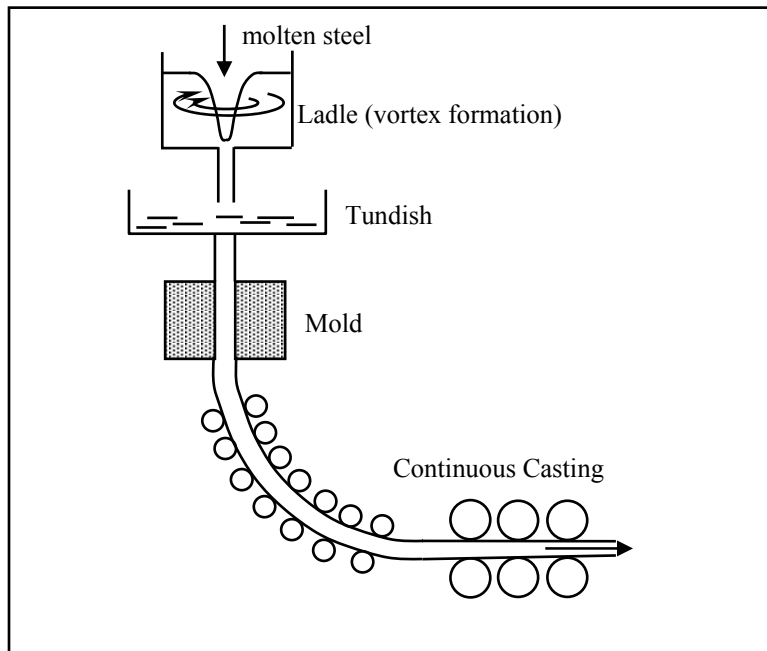


Figure 1.2: Continuous Casting Process

1.4.1 Two types of gravity-driven drainage

Each of the four vessels used in the continuous casting process is drained under gravity-driven conditions, as seen in Figure 1.2. However, two types of gravity-driven drainage are involved. *Batch-type drainage*, where the head of liquid steel in the vessel decreases throughout the drainage process, is used in the tapping of BOF's and EAF's, in ladle teeming, and in tundish pouring during ladle changes. *Constant-head drainage* occurs in the tundish, except at ladle changes, and in the mould. While batch-type drainage is definitely a non-steady state process, the constant-head drainage encountered in typical steelmaking tundishes and moulds can be described as quasi-steady state, if not truly steady-state process.

1.4.2 Geometry and dimensions of continuous casting vessels

The geometry and dimensions of the four vessels differ considerably from one another. While the cylindrical BOF converter remains vertical during the blowing period, it resembles a horizontal cylinder, quite akin to *bath-tub*, while it is being tapped. The ladle is essentially a vertical cylindrical vessel, with a centrally positioned teeming nozzle on the bottom. Moulds are usually straight, vertical-walled vessels with identical entrance and cross-sections. Tundishes are of different shapes, ranging from the simple rectangular, sloped-wall troughs to T-shaped tundishes, Delta-shaped tundishes etc.; the number of nozzles on the floor of the tundish and the physical dimensions of the tundish depend on the shape, the dimensions, and the number of strands or slabs or blooms to be produced.

1.4.3 Tangential velocity distributions in various vessels

It is almost impossible to avoid the presence of adventitious residual tangential velocities in any of the above mentioned four vessels. It is even difficult to predict the magnitude and direction of rotation of such tangential velocities. Velocity distributions in the BOF converter can be affected by the blowing conditions, reaction behavior, thermal gradients, etc. As for the initial tangential velocities in the ladle, the controlling variables include the furnace tapping rate, the angle of entry and relative location of the tapping stream within the ladle, any rotational velocity components generated by subsequent secondary metallurgical operations, the period of time (holding time) that the liquid steel is simply held in the ladle prior to start of ladle teeming on to the tundish, and even the rotational motion imparted to the liquid steel while the ladle is brought into the casting position on the continuous casting machines turret. Moreover, the tangential velocity distribution in the ladle can be affected by the ladle teeming itself, coupled with the ladle and nozzle geometries.

The residual tangential velocity distributions in the tundish are far more complicated. Various factors like tundish geometry and the relative location of the impinging ladle stream, the presence or absence of flow modifying devices like the pouring box, dams and weirs, the instantaneous head of liquid steel in the tundish etc. Even though some mathematical models have predicted the tangential velocity distributions in the tundish, it is extremely difficult to predict the critical liquid heads for vortexing funnel formation from them.

The situation in the moulds is also quite complicated. In addition to the geometry of the mould itself, a number of other factors can affect the tangential velocity distribution. The presence or absence of submerged entry nozzle (SEN), the port angle of the SEN, the relative

location and depth of immersion of the SEN beneath the steel-slag interface, mould powder conditions, etc., have an influence on the tangential velocity distribution in the mould.

1.5 IMPLICATIONS OF SLAG ENTRAINMENT

The necessity of prevention of slag entrainment during each of the four liquid steel transfer operations will be clear when the harmful effects of such entrainment on the cleanness of cast steel, chemistry and temperature of liquid steel, productivity, and yield are highlighted. The prevention of slag entrainment thus has quality as well as cost benefits.

1.5.1 Metal Cleanness

Ever increasing amounts of high grade steels are being continuously cast. This trend is expected to increase well into the future and with it the need to produce steels with higher levels of internal cleanness. Due to their detrimental influence on the physical and mechanical properties, it is desirable to limit the number of large inclusions. For example, inclusions tend to decrease deep-drawability, and affect the surface quality of exposed automotive and appliance sheet.

Inclusions in continuously cast steel are essentially oxides of Al, Ca, Mg, and Si with traces of Mn, Na, S, P, etc. Inclusions are often classified as indigenous or exogenous, so as to reflect the dependence of their origins on both physical and chemical events inherent to various steel processing operations. Inclusions that are formed due to reoxidation, deoxidation, and desulphurization reactions are usually considered indigenous to steelmaking while entrained slag inclusions are not. Considerable knowledge is available on the prevention of indigenous inclusion formation; for example, effective inert gas shrouding of liquid steel streams from the ladle and tundish can prevent reoxidation to a large extent; argon bubbling in the ladle is effective in floating out a large portion of the deoxidation and desulphurization products. However, efforts to minimize exogenous inclusions are limited by the dearth of information on slag entraining funnel formation.

Slag entrainment is also known to cause reoxidation of the metal, the removal of which is bound to result in the generation of additional indigenous inclusions. Entrainment of ladle slag has been observed to result in a steady increase in the volume of slag in tundish, as sequence casting progresses, and it is reported that the inclusion content of the cast slabs is directly proportional to the tundish slag thickness. Vortex formation is also known to cause slag entrainment whenever the steel level in the tundish drops below a critical value.

Clearly, the formation of slag entraining vortex funnel contributes directly, as well as indirectly, to an increase in the number of exogenous, as well as indigenous, inclusions in cast products, and must be avoided during all stages of liquid steel transfer.

1.5.2 Productivity

The overall cost of production is dependent on the productivity and yield, among other factors. Measures needed to counteract the effects of slag entrainment, e.g. longer duration of argon bubbling in the ladle, result in increases in processing time, and in the amount of expensive additives like deoxidants, desulphurizing agents and alloying additions. Entrainment of ladle slag also reduces the life of tundish refractories.

1.5.3 Yield of Liquid Steel

It is usual practice in steelmaking to stop the drainage of liquid steel from the continuous casting vessels sufficiently early, before the vessel is completely empty of liquid steel, so as to avoid having to deal with the problems caused by potential slag entrainment. It is reasonable to estimate the liquid steel yield losses associated with a need to prevent slag entraining funnel formation at about 1 to 3 tons per converter, 5 to 10 tons per ladle, and 10 to 20 tons per tundish. Thus the minimization of yield losses due to slag entraining funnel formation is of paramount importance to steelmakers.

1.5.4 The End of Drainage Decision

The successful prevention of slag entrainment depends on the timing of the decision to stop the vessel drainage. The end of drainage decision is one of compromise- it is impossible to maximize quality without sacrificing yield and /or productivity, or vice versa. If liquid steel transfer is stopped too early, the yield will suffer; too big a delay in stopping drainage will result in slag entrainment. It is generally accepted that the effective prevention of slag entrainment does depend on the ability to master three mutually independent sub-tasks, *viz.*, suppression of slag entrainment mechanisms, accurate detection of slag flow, and minimization of time delay between the detection of slag and the actual end of drainage, respectively.

1.6 OBJECTIVES OF THE PRESENT WORK

The overall goal of the present study was to develop a fundamental understanding of vortexing funnel formation, as prevalent in steelmaking process. For the sake of simplicity, it was decided to limit experiments to batch-type ladle drainage. In other words, it was decided to neglect the roles played by vessel geometry and drainage modes. Further, instead of attempting to

geometrically scale any given industrial ladle, tests were performed in two ladles of different diameters.

The primary independent variable independent variable in the experiments was the initial tangential velocity possessed by the primary liquid in the ladle at the instant drainage was instigated. The chosen inflow configuration (discussed in Chapter 3) produced a residual tangential velocity distribution that was more or less independent of radial, azimuthal and axial positions.

1.7 STRUCTURE OF THE REMAINDER OF THE THESIS

The remainder of the thesis is divided into chapters that are devoted to each part of the current study. Chapter 2 is devoted to discussing the current knowledge of the phenomenon and the hydrodynamic principles of vortex formation. Chapter 3 discusses the experimental setup and procedure adopted in performing the scale model experiments. Chapter 4 is dedicated to describing the numerical model and predicted results obtained from the numerical model. Scale modeling approach and scaling laws formulations are explained in chapter 5. The results obtained from experiments are discussed and compared with the numerical results in chapter 6. In closing, chapter 7 states the concluding remarks and the future work.

CHAPTER 2

LITERATURE REVIEW AND THEORETICAL BACKGROUND

2.1 CURRENT UNDERSTANDING OF SLAG ENTRAINING FUNNEL FORMATION

In the past few years, researchers have invested a considerable amount of time and energy in clarifying our understanding of the slag entraining funnel formation with particular emphasis on the critical liquid steel heads from which the vortexing and non-vortexing funnels are formed. Despite significant advances in the understanding of the phenomenon, a number of questions still remain unanswered.

Hammerschmid *et al.* [1] studied vortexing funnel formation in three different ladles, the primary liquid being water in two ladles and mercury being the primary liquid in the other. In these experiments, the ladles were filled with tangentially disposed inlet which induced rotational motion in the liquid. The V_θ at one location in the 1190 mm diameter ladle was measured as a function of holding time (the period between the end of filling and the start of emptying). Since V_θ decreased with increasing holding time, the vortexing funnel formation data was expressed as a function of holding time. Thus, it was found that $H_{cr,v}$ decreased as the holding time increased; i.e., it was implicitly understood that $H_{cr,v}$ was directly proportional to the intensity of rotational motion possessed by the liquid at the beginning of drainage. Similar results were also obtained during the teeming of mercury from a 240 mm diameter ladle.

In the third ladle, of internal diameter 510 mm, Hammerschmid *et al.* found that $H_{cr,v}$ varied inversely with the diameter of the nozzle, i.e., the smaller the nozzle diameter d , the larger was $H_{cr,v}$ for otherwise identical initial conditions. It was also found that the relocation of the drainage nozzle from the central axis to an eccentric (off-central) position, resulted in a dramatic decrease in $H_{cr,v}$, all other conditions remaining the same.

Despite having studied vortexing funnel formation in three different vessels, Hammerschmid *et al.* did not summarize their results in a single plot, e.g. correlating $H_{cr,v}$ to the initial tangential velocity, probably because the relationship between the holding time and the residual tangential velocity distributions in the individual ladles were not quantified. In the absence of such knowledge, the question that needs to be answered is whether, or not, one would have to rely on full-scale experiments.

In full-scale water model experiments, Andrzejewski *et al.* [2] found out that a non-vortexing funnel always formed at the end of the drainage, whether it has been preceded by a

vortexing funnel, or not. Reasonable agreement was obtained between the water model and a theoretical model.

It must also be noted that the critical height of non-vortexing funnel formation is independent of the initial liquid depth, the vessel diameter, and the physical properties of the liquid. Andrzejewski *et al.* assumed that the ladle steel possessed negligible angular momentum and concluded that the slag entrainment is due to the non-vortexing funnel formed at the end of drainage and there is no role played by the vortexing funnel formation. Hence, efforts to minimize slag entrainment must be directed towards stopping drainage prior to, or immediately after, the initiation of a non-vortexing funnel formation. Harleman *et al.* [3] considered the problem of selective withdrawal from a vertically stratified fluid consisting of an upper and lower liquid layers differing slightly in density and found out that the rate of flow greater than the critical discharge causes increasing amounts of upper liquid to be drawn into the intake. The magnitude of the critical discharge is determined in terms of the dimensionless variables defining the liquid and geometric properties. The vertical density gradients may occur due to temperature differentials, suspended sediment loads or dissolved salt content. In these experiments, water solutions of sodium chloride were used for the lower liquid and fresh water for the upper.

Ramani Sankaranarayanan and R.I.L. Guthrie [4, 5, 6, 14] carried out a fundamental study to elucidate the parameters that influence the critical limiting height below which a vortexing funnel formed during ladle teeming operations. They concluded that given the right conditions, i.e. rotational motion with its axis of rotation aligned with the axis of drainage nozzle, a vortexing funnel can be initiated from very large liquid heads. The critical limit of vortexing funnel formation is independent of vessel dimensions and to a certain extent the vessel geometry as well. Given that adventitious tangential velocities are inevitably present in ladles and tundishes, prior to the and during teeming operations, the possibility that very tall vortexing funnels can be initiated quite easily is a major cause of concern. Since teeming is a gravity-driven process that is essentially independent of liquid density, there is a strong likelihood of vortex formation in liquid steel being quantitatively similar to that in water. Numerical computations indicated that both water and steel would exhibit identical behavior as far as decay in initial tangential velocities (prior to the beginning of teeming) is concerned, provided the initial conditions are the same. An oil entraining vortex was found larger than the air entraining vortex (under similar conditions), and oil has a density closer to water than compared to air. This

leads to the conclusion that fluid slag would increase the chances of vortex formation in liquid steels. It was thus concluded that slag entrainment in ladle teeming can be attributed to a vortex-sink type vortex but the need to effectively model the vortex formation with slag entrainment phenomenon and the subsequent attempts to prevent the formation of vortex still remains.

Chang [7] performed a review of papers on vortices formed in cylindrical tanks with a drain outlet at the centre of the bottom of the tank. He concluded that no theoretical treatment exists to fully explain the spatial and temporal variations of vortex parameters. R.I.L. Guthrie [8,9] stressed on the development of ladle metallurgy and the contributions of mathematical and physical models to the understanding and control of the slag entrainment phenomenon. D. Mazumdar [10] carried out extensive computer predictions to study the flow and particle motion during central gas injection into cylindrical vessels. K. Hyoungbae [11] studied the formation of a late rotating vortex over an off-centre drain nozzle and found out that the sloped bottom ladle could be beneficial in terms of steel yield. Jewasinski and Sucker [12] reported that the use of stopper rod positioned above the drainage nozzle of ladle could suppress vortexing funnel formation, particularly when the diameter of the stopper rod was three times larger than the nozzle diameter. Their experimental setup was similar to that of Sucker *et al* [13]. However, the formation of a vortexing funnel away from the axis of the stopper rod has been reported by other workers [15, 16, 17, 18]. Thus the protection offered by stopper rods is not universally accepted.

2.2 THEORETICAL BACKGROUND

2.2.1 Vorticity and Circulation

These are two distinct but related quantities associated with any moving fluid which is not necessarily rotating.

The vorticity ζ of a fluid element is mathematically defined as:

$$\zeta = \text{curl } \mathbf{V}$$

and so is a vector quantity related to velocity gradients in the region of the element of the fluid.

In physical terms, the vorticity is a measure of the tendency of the fluid element to turn about its own axis as a result of non-uniform velocity distribution.

Consider an imaginary cross-shaped marker whose arms are free to turn independently of one another. If this is placed in an ideal fluid, flowing with uniform velocity distribution, the cross will suffer no distortion or net rotation from its initial orientation, showing there is no vorticity in that region of the fluid.

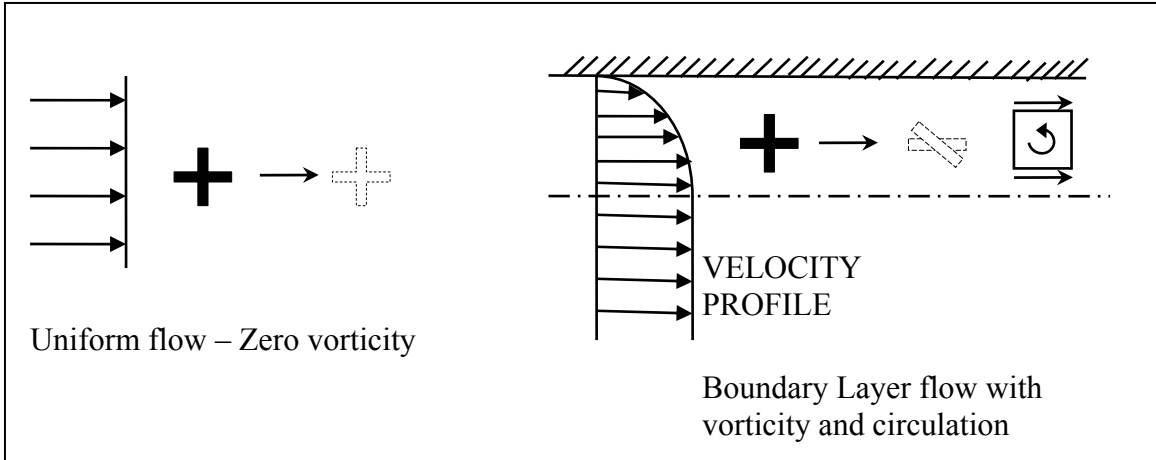


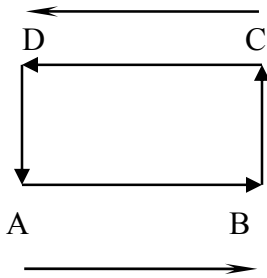
Figure 2.1: Vorticity and Circulation

However, consider the flow in a real fluid near a solid boundary. The velocity distribution is non-uniform as shown and whilst the horizontal arm is unchanged, the vertical arm of the cross rotates from its initial position due to the varying velocity across it. Thus there is a net rotation of the cross showing the existence of a vorticity component in the boundary layer region in a direction perpendicular to the plane of the paper. The circulation also has a non-zero value in this case.

Circulation, on the other hand, is a scalar quantity and is defined as the line integral

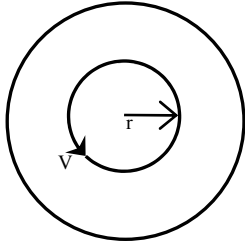
$$\text{Circulation } \Gamma = \oint_L V \cdot dS \quad (2.1)$$

The integral is taken around any arbitrary closed curve drawn within the fluid. Take the simple case of uniform velocity V and the curve L as a rectangle as shown, then



$$\begin{aligned} \Gamma &= \oint_L V \cdot dS \\ &= \int_{AB} V \cdot dS + \int_{BC} V \cdot dS + \int_{CD} V \cdot dS + \int_{DA} V \cdot dS \\ &= V \times AB + 0 + (-V) \times AB + 0 \\ &= 0 \end{aligned}$$

For a two dimensional circular motion, Γ at radius r can be found by taking V to be the tangential velocity and the curve L to be a circle of radius r . Then Eq. (2.1) becomes



$$\Gamma = V \cdot 2\pi r$$

The relationship between vorticity and circulation can be derived from Stokes' theorem and is found to be

$$\Gamma = \int_S \zeta \cdot dS$$

Where S is any area within the fluid bounded by the curve L . Thus, where there is a local region of zero vorticity, the local circulation is also zero.

For a free vortex, the circulation round any curve which does not include the origin is zero since vorticity is also zero. However, if the origin is also included, the circulation is no longer zero.

2.3 HYDRODYNAMIC PRINCIPLES OF VORTEX FORMATION

The flow associated with a typical vortexing funnel formation is a three-dimensional, unsteady, viscous, initial condition-dependent flow that does not have a complete mathematical or numerical solution. Many mathematical analyses have been built upon the potential vortex theory which is an idealized flow situation assumed to be inviscid and steady, radial and axial velocity components in the infinitely large vessel being zero. The surface streamlines of a potential vortex are logarithmic spirals, and the free surface of the potential vortex is hyperboloidal in shape. Some insights can be gained from such mathematical analyses. However, the fact remains that current hydrodynamic theory cannot yet provide steel-mill workers the information on the liquid head from which a vortexing funnel will form. The aim of this chapter is to provide an overview of vortex formation based on the conservation of angular momentum, free and forced vortices.

2.3.1 Principle of Conservation of Angular Momentum

Andrade, in 1936, stated that one would have to take into account the principle of conservation of angular momentum while considering the origins of the "vortex" in *bath-tub*. As an example

of conservation of angular momentum, he cited the case of a dancer who wanted to spin very fast. She would have to get up as great spin as possible with her arms out, so that when she subsequently dropped her hands she could start spinning faster. Thus Andrade hypothesized that “when a particle of water circulating around an axis alters its distance from that axis, it must change speed so that the product of distance by speed remains constant- the closer it comes, the faster it must move, and, still more, the greater the number of revolutions per second, since, the distance being less, the angular velocity would have to increase if the velocity had to remain the same.” The principle of conservation of angular momentum can be written as follows:

$$mV_{\theta}r = \text{constant} \quad (2.2)$$

Where m , V_{θ} , r are the mass, initial tangential velocity, and radial position of the particle rotating about the axis at $r = 0$.

2.4 FREE AND FORCED VORTICES

2.4.1 Free Vortex

The angular momentum of a free vortex in an ideal, incompressible and inviscid liquid is conserved. Thus, in keeping with Eq. (2.1), the tangential velocity distribution of a free vortex can be described as

$$V_{\theta} = \frac{K}{r}$$

Where r is the radial coordinate and K is the strength of the vortex. K is usually defined as the product of $V_{\theta} \cdot r_0$, V_{θ} being a known reference value of tangential velocity at a radial location, $r = r_0$. K is also a measure of the prevalent liquid circulation, Γ , since by definition,

$$\Gamma = 2 \pi K$$

Thus, the circulation of a free vortex is constant, as long as the path over which it is measured encompasses the vortex core. However, the circulation can be shown to be zero for any path that fails to encompass the vortex centre. In other words, the free vortex is everywhere irrotational except at the centre. Alternately, a fluid particle, or a marker, that is introduced into the vessel at the periphery will travel through the centre without ever rotating about its own axis. Once it reaches the central axis, however, it would spin rapidly and descend into the exit nozzle. The distribution of angular velocity, ω , in *radians/second*, in the free vortex can be written in terms of the rotational speed, f , in *revolutions/second* as follows:

$$\text{Free vortex: } \omega = \frac{f}{2\pi} = \frac{V_\theta}{r} = \frac{K}{r^2}$$

2.4.2 Forced Vortex

The case of an ideal liquid whose angular velocity, ω , is constant is usually referred to as a forced vortex,

$$\text{Forced vortex: } \omega = \frac{f}{2\pi} = \frac{V_\theta}{r} = \text{constant}$$

Where the vorticity is everywhere greater than zero. Rigid body rotation is an extreme case of forced vortex motion, where the vorticity is constant and equal to twice the angular velocity. Fluid particles moving around a common axis in circles, *i.e.* as a rigid body, would rotate about their own axes once every revolution, much like the moon does on its travel around the earth, always showing the same face to those on earth. Rigid body rotation can be produced in a liquid holding vessel by rotating the vessel about its own axis, for a time period long enough for steady state conditions to be reached. The liquid would assume the shape of a paraboloid.

The equations for the free vortex and forced vortex can be combined into a single equation as follows:

$$V_\theta = \frac{\text{constant}}{r^n}$$

Where $n = 1$ for a free vortex

$n = -1$ for a forced vortex

A major proportion of the vortexing funnels encountered in practice are likely to have a value of n that varies between -1 and 1.

2.5 Vortex plus Sink-logarithmic spiral surface flow lines

The classical potential vortex is obtained as the superposition of a line vortex and a line sink, both of which share a common centre, or axis. It is assumed that the liquid is incompressible and inviscid, and that two-dimensional flow is steady. The liquid head in the infinitely large vessel is maintained constant, presumably by a continuous inflow of liquid, introduced into the vessel far away from the drainage exit, and equal in magnitude to the outflow. Naturally, it is assumed that the viscous forces are absent and that all body forces are conservative.

A line vortex and a line sink are graphically shown in Figure 2.2. The radial and tangential velocity distributions for a line sink are given by

$$V_{r,sink} = \frac{m}{r} \quad V_{\theta,sink} = 0$$

Where the sink strength m has a negative value. The sink streamlines flow in towards the central axis. The stream function ψ and velocity potential ϕ for the line sink are given by

$$\psi = m\theta \quad \phi = m \ln r$$

The roles of ψ and ϕ are reversed in the case of a line vortex,

$$\psi = -K \ln r \quad \phi = K\theta$$

where the vortex strength K has the same units as the sink strength m , namely, velocity times length. The radial and tangential velocity distributions for the line vortex are given by

$$V_{r,vortex} = 0 \quad V_{\theta,vortex} = \frac{K}{r} \quad (2.3)$$

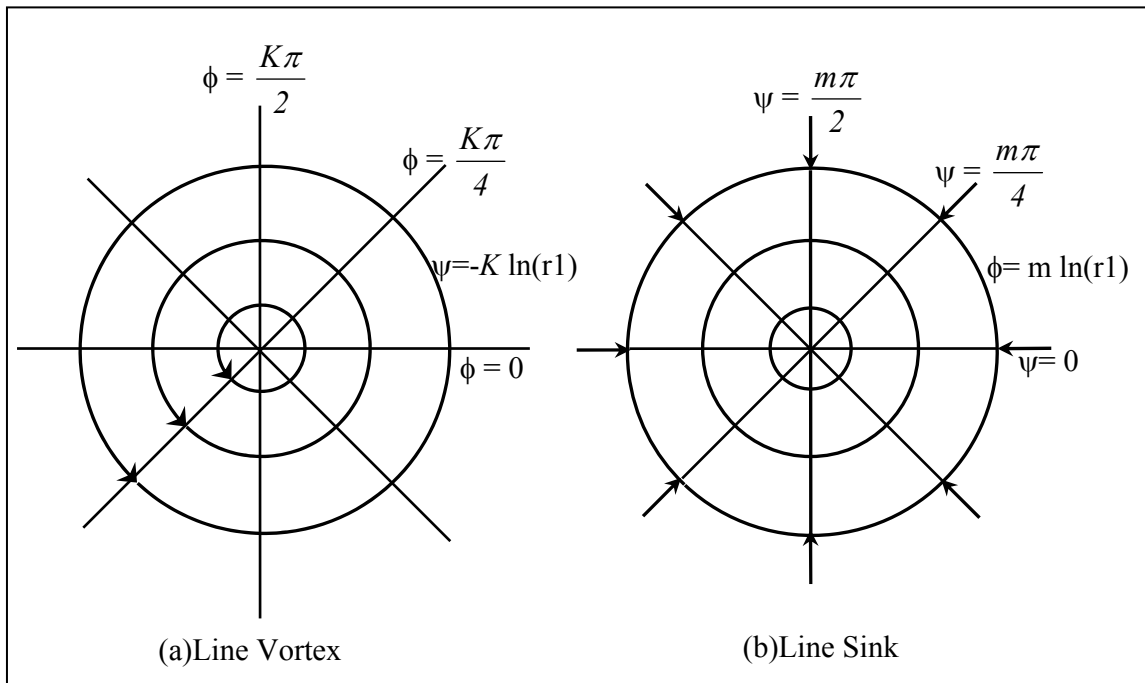


Figure 2.2: Graphical representation of a line vortex and a line sink

Note that both the sink and vortex have singularities at the centre, where both the ψ and ϕ are undefined, and the velocities (V_r in the case of sink and V_θ in the case of the vortex) are infinite. The velocity distributions for the line sink and the line vortex are both incompressible and irrotational.

Stream functions and velocity potentials of superposed plane flow solutions are additive. In other words, the stream function of the combined vortex-plus-sink can be obtained by adding

together the individual stream functions of the vortex and the sink. Likewise for the velocity potential. Thus, the stream function and velocity potential of the vortex-plus-sink are given by

$$\psi = m\theta - K \ln r \qquad \phi = m \ln r + K\theta$$

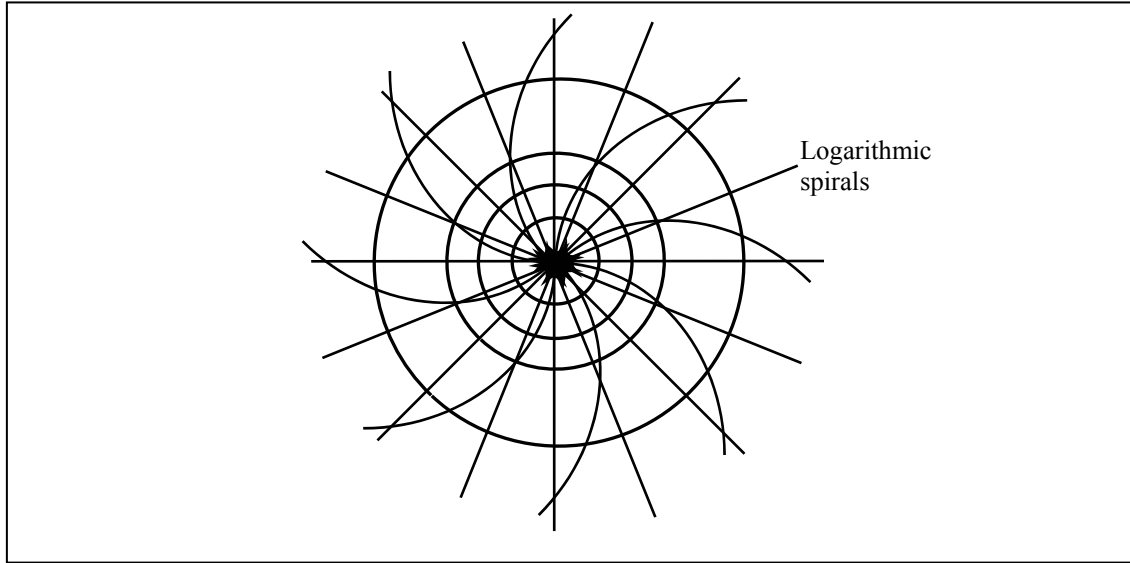


Figure 2.3: Streamlines for a vortex plus sink constructed by a graphical method

2.6 THE SURFACE PROFILE OF THE POTENTIAL VORTEX

A limiting case of the potential vortex, or vortex-plus-sink, is the case where the sink strength m is negligibly small. The surface profile for this situation can be determined easily by applying the standard Bernoulli analysis. Thus, we start with the assumption that the velocity distribution of the potential vortex is given by $V_r = 0$, $V_\theta = K/r$. Note that the justification for this assumption follows, for example, from Shapiro's [19] observation in the sink-vortex tank of a spiral flow line that was sufficiently tight for it to be approximated by a set of concentric circles. Also note that the velocity distribution chosen is identical to that of the line vortex, Eq. (2.3) (for line vortex) substituting this velocity distribution in the steady-state irrotational energy equation, or the Bernoulli equation, we obtain

$$p + \rho K^2 / 2r^2 + \rho g z = C$$

Where C is a constant. It can be shown that a surface of constant pressure must have the shape

$$z|_{p=p_1} = C_1 - K^2 / 2gr^2 \qquad C_1 = \frac{C - p_1}{\rho g} \qquad (2.4)$$

Thus, all constant pressure surfaces, including the free surface where the pressure is equal to atmospheric pressure, have the form of a second order hyperboloid, i.e. z varies inversely with r^2 . Note that Eq. (2.4) indicates that the depression in the centre of the vortex will be infinitely deep.

Shapiro [19] found for large values of circulation, the tail of the vortex dropped out of sight, almost as if it extended to infinity. However, when the flow rate, and the circulation, were reduced it was found that the tail of the vortex shrank back to become a mere dimple in the limiting case. Thus, it is usually considered that a small rotational core forms at the axis which reduces the depth of the vortex depression.

2.7 RANKINE COMBINED VORTEX

The well-known hydrodynamist Rankine was amongst the first to suggest that infinite velocities could not possibly be present at the axis of the line vortex. Rankine thus proposed that a line vortex should consist of a central region of constant vorticity (as in rigid body rotation) surrounded by a free vortex with a constant circulation to match that at the outside limit of the central region. Thus, if the radius of central region was a , one would obtain the following tangential velocity distribution:

$$V_{\theta} = \omega r \quad 0 \leq r \leq a$$

$$V_{\theta} = \frac{\omega a^2}{r} \quad r \geq a$$

The velocity distribution and surface profile of a Rankine combined vortex are shown Figure 2.4. It can be seen that increasing the vorticity (*i.e.* increasing the angular velocity ω), or decreasing a leads to an increase in the depth of surface depression until eventually an air-core forms (*i.e.* h_0 becomes zero).

It must be noted that the Rankine combined vortex differs from the potential vortex in only one aspect; while the singularity at the axis is avoided, every other assumption of potential vortex theory is held valid, including inviscid flow, zero axial and radial velocities, infinitely large vessel, each of which is not entirely true. Even the requirements that steady state conditions be prevalent in the holding vessel may not be met in practical conditions. Thus, although it may not provide greater insights into the real- world phenomenon, it can be used to arrive at certain basic conclusions about the flow *i.e.* whether it follows a standard vortex pattern or not.

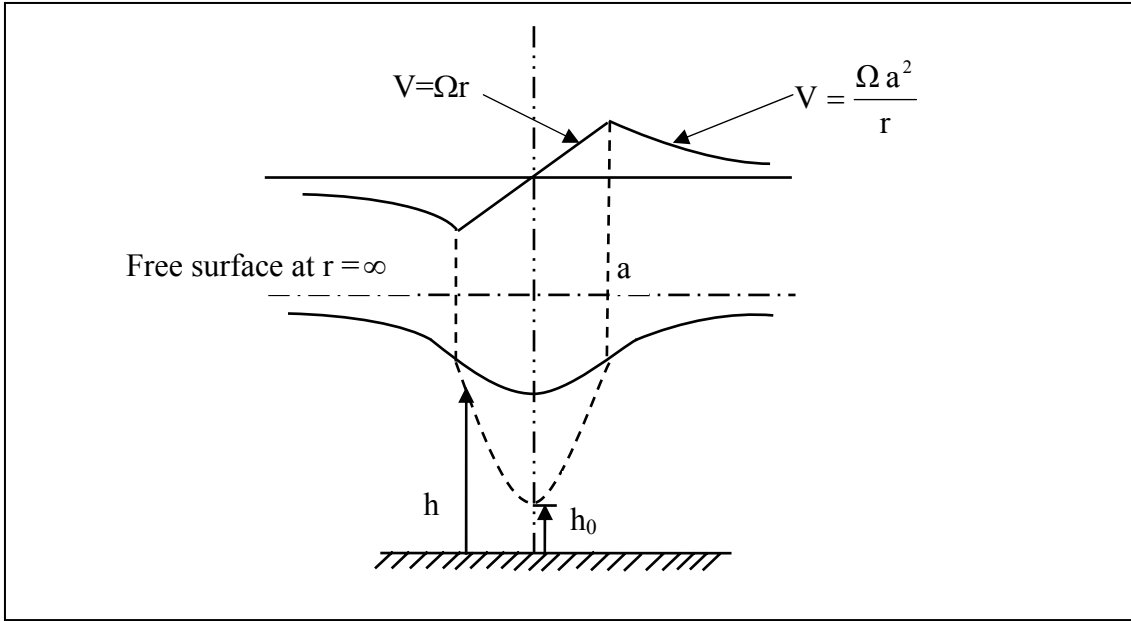


Figure 2.4: Rankine combined vortex

CHAPTER 3

EXPERIMENTAL PROCEDURE

3.1 EXPERIMENTAL SETUP

Two different size scale models were designed in this study. The large scale model consists of 254 mm inner diameter \times 254 mm height plexiglass cylinder with a 7.62 mm inner diameter nozzle attached to the center of the bottom plate for draining liquid. The small scale model consists of 127 mm inner diameter \times 127 mm height plexiglass cylinder with a 3.81 mm inner diameter nozzle. Figure 3.1 shows detailed dimensions of these two scale models and their side-by-side photograph.

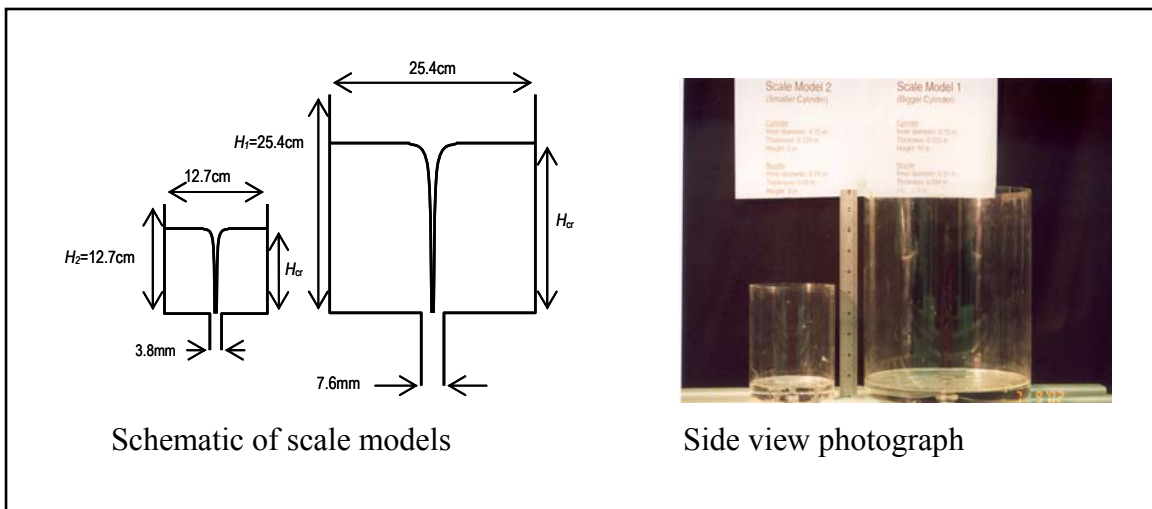
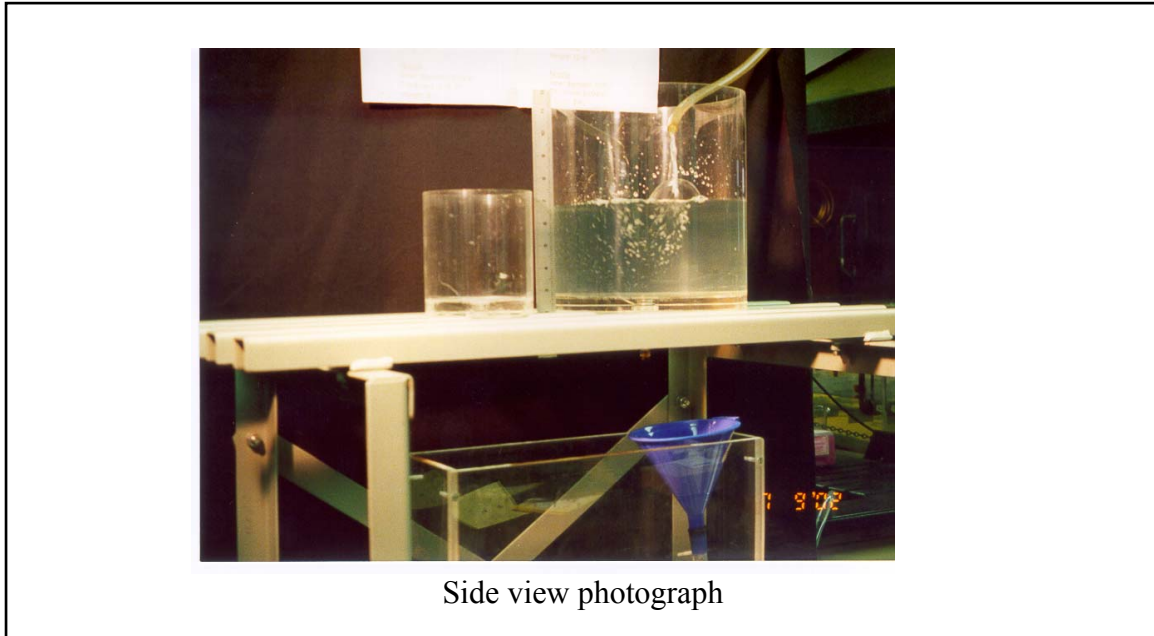


Figure 3.1: Schematic of scale models and photograph

The experimental setup consists of the two scale models fitted with nozzle at the bottom, the water inlet and the water outlet setup as shown in Figure 3.2. The cylinders are mounted on a fixed stand that is placed on the worktable. It is verified that the cylinder surface is perfectly horizontal by placing a spirit level on the base of the cylinders. A rubber pipe fixed at one end to an external water source (wash basin) is suspended with the open end in the cylinder at an angle so that the water hits the cylinder wall with an initial rotational motion. The rubber pipe can be moved out of the cylinder after the water level has reached the top. A rubber stop ensures that the water remaining in the pipe does not flow out after removal from the cylinder. The outlet consists of a plastic funnel that collects the water exiting from the nozzle and a pipe fixed to the end of the funnel carries the water to a discharge bin. A rubber stop press fitted to the nozzle ensures that the water does not exit the cylinder during filling and before the experiment is started.



Side view photograph

Figure 3.2: Experimental setup

3.2 PRELIMINARY OBSERVATIONS

Before carrying out the detailed experiments using PIV techniques, an initial round of experiments were done using food color. The aim of these experiments was to study the causes of vortex formation. Two sets of experiments were done. In the first set, the cylinders were filled with water to the top and the nozzle was opened only after the water was perfectly still, i.e. there was no velocity in any direction. A small syringe was used to place 2-3 drops of food color on the receding water surface. As the water level decreased, it was observed that the food color had no movement on the surface, i.e. there was no horizontal motion of fluid particles during emptying in the absence of initial rotation. The water level receded at constant speed and right before the drainage ended, the food color was drawn towards the nozzle in the radial direction suggesting a drain sink phenomenon.

The same experiment was performed with initial rotational motion to the water. In this case, there was a movement of the food color in the form of concentric circles around the centre of the cylinder. After some time, a vortex begins to appear which reaches the bottom after a few seconds. The movement of food color in the presence of a vortex was in the form of concentric circles that had a spiral type motion and were drawn into the vortex core before exiting through the nozzle. This is shown in Figure 3.3 and confirms that the initial tangential velocity of water is responsible for vortex formation. Furthermore, the vortex formation causes a resultant motion in

the horizontal direction into the centre of the cylinder that causes entrainment of the floating surface on top into the nozzle.

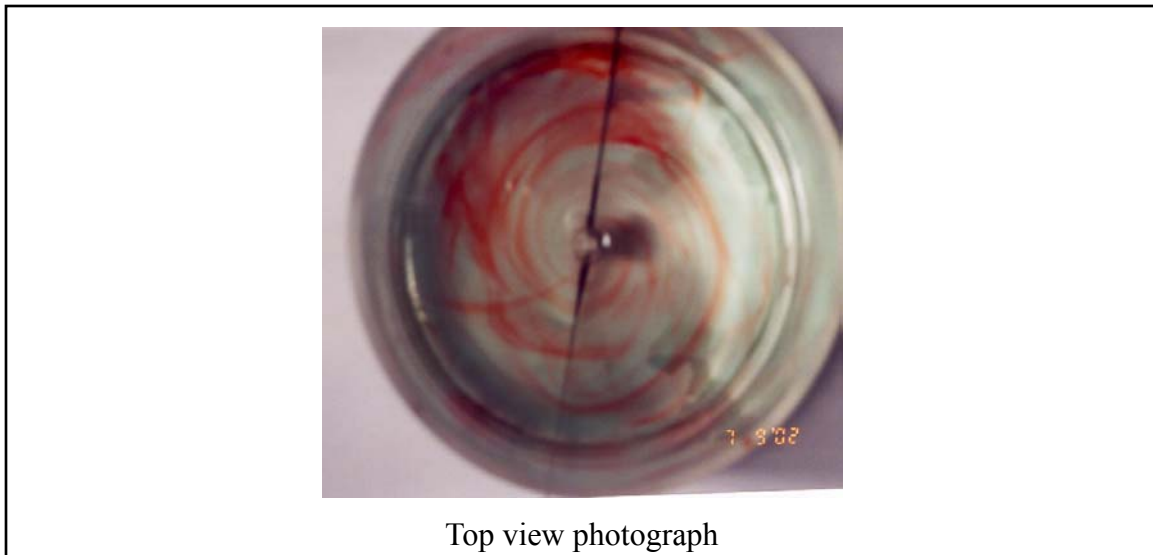


Figure 3.3: Surface profile observed using food color (in the presence of vortex)

3.3 EXPERIMENTS USING PARTICLE IMAGE VELOCITOMETRY

The model experiments using food color confirmed that the initial tangential velocity is responsible for vortex formation and the subsequent slag entrainment during steel teeming process. To further understand the characteristics of this initial tangential velocity and its influence on the critical height of vortex formation (the height at which the vortex becomes fully developed, i.e. reaches the base of the cylinder), experiments were performed using the Particle Image Velocitometry technique to measure the initial tangential velocity and critical height.

3.3.1 Principle of PIV

PIV system measures velocity by determining particle displacement over time using a double-pulsed laser technique [20]. A laser light sheet illuminates a plane in the flow, and the positions of particles in that plane are recorded using a digital or film camera. A fraction of a second later, another laser pulse illuminates the same plane, creating a second particle image. From these two particle images, unique and robust PIV analysis algorithms obtain the particle displacements for the entire flow region imaged, and give velocity information at different locations quickly and reliably. Figure 3.4 shows typical side images of the vortex in the experiments using a digital video camera and PIV. The seeding particles are seen as the white colored dots and these are Aluminium oxide spheres of diameter $0.3\mu\text{m}$.

Image capturing during the teeming scale model experiments using PIV and a digital video camera were conducted in the following manner.

(1) The laser beam is adjusted such that the beam strikes the cylinder in the horizontal direction (Figure 3.5) at a height corresponding to the initial height of the liquid level.

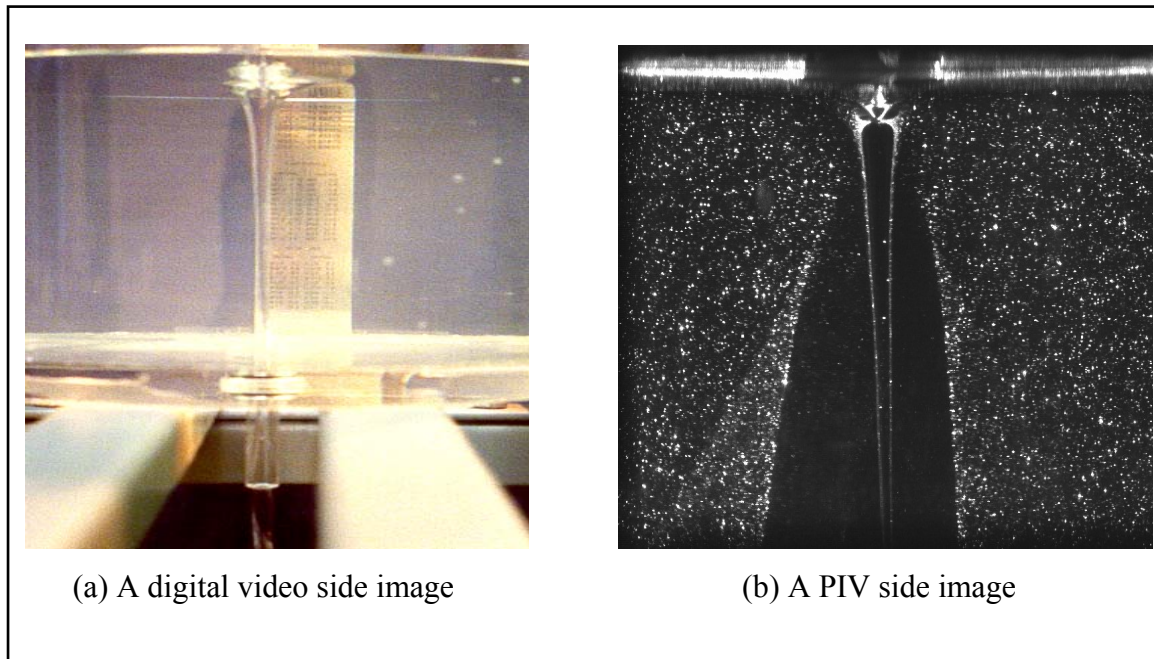


Figure 3.4: Image capturing using Digital camera and PIV

(2) The cylinder is filled with water and seeding particles are immersed.

(3) An initial tangential velocity is imparted to the water by stirring along the circumference using a long wooden stirrer. The initial tangential velocity was controlled by imparting various stirring speeds and also the waiting time before the nozzle was opened. This process ensures uniform distribution of seeding particles in the cylinder.

(4) The frequency of laser beam and the location of a CCD camera were adjusted to obtain a clear and high resolution CCD image that captures the horizontal plane of rotating water illuminated by the laser beam corresponding to the initial height.

(5) A color digital video camera looking at side view of scale models recorded an entire teeming process. From the recorded image, the critical liquid height at which the tip of vortex reaches the bottom of cylinder was measured.

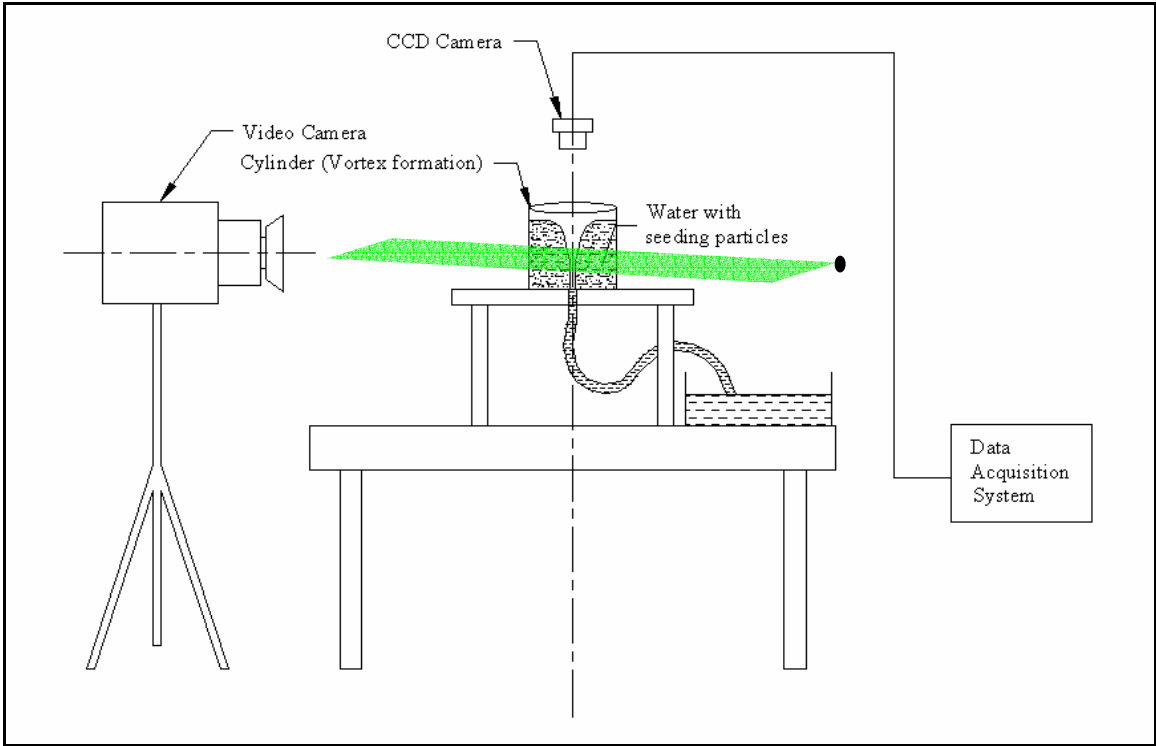


Figure 3.5: Experimental setup with PIV (horizontal laser beam)

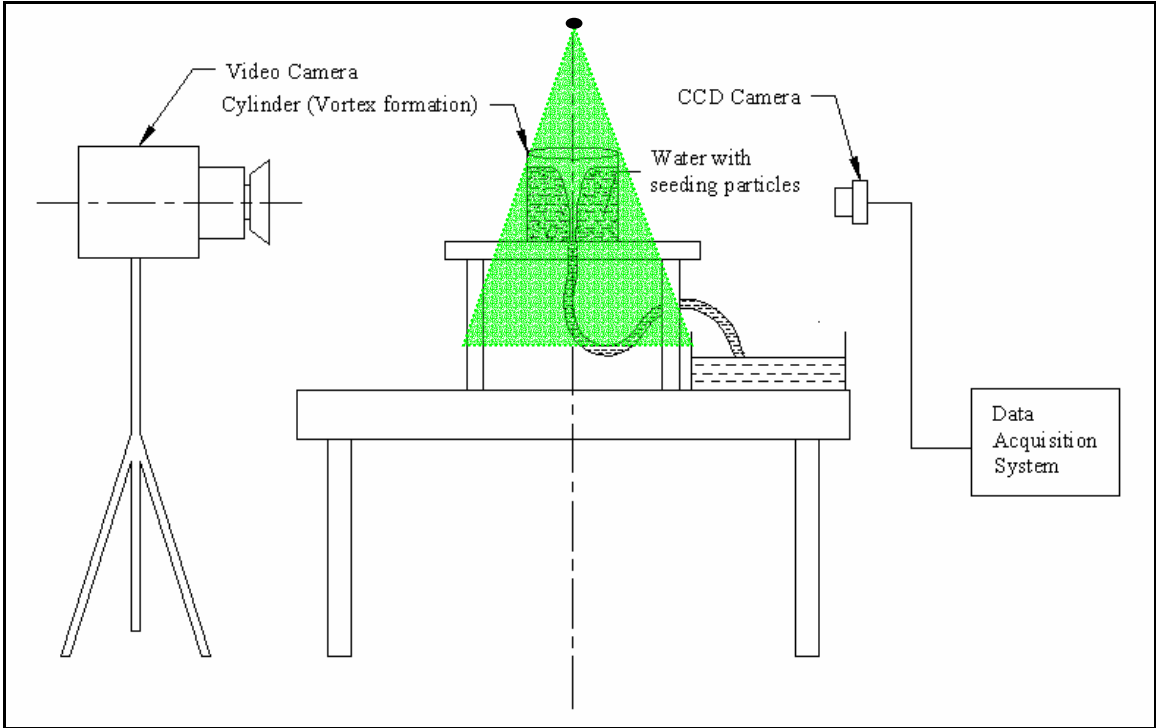


Figure 3.6: Experimental setup with PIV (vertical laser beam)

Once the tangential velocity is imparted to the water, the laser is applied and the water flow field is recorded by the data acquisition system. At the required initial tangential velocity, the nozzle is opened and the video camera is activated simultaneously. As the liquid level starts dropping, a vortex might appear after sometime if the initial tangential velocity is high enough. At the instant the vortex appears, the critical height is achieved. Hence, for a particular initial tangential velocity, the critical height can be determined from a single run. Several runs are made with various initial tangential velocities and the corresponding critical heights are noted.

The PIV images of vertical plane (Figure 3.6) of the cylinder were also taken to obtain axial and radial velocities at different heights. Figure 3.4 shows typical digital video and vertical PIV images of the vortex observed. A number of runs ensure that the critical heights vary from the highest to the lowest. The same procedure is adopted for both big and small scale models. The experimental observations and results are discussed in the following chapters.

CHAPTER 4

NUMERICAL MODELING

4.1 INTRODUCTION

A CFD package, Fluent (Fluent Inc.), was applied to simulate fluid motion during the teeming process. The model is based on transient, two-phase (water and air), 2D (axisymmetric) fluid flow. The Volume of Fluid (VOF) model is adopted to simulate water and air flows. The VOF model relies on the fact that two or more fluids (or phases) are not interpenetrating. For each additional phase added to the model, a variable is introduced: the volume fraction of the phase in the computational cell. In each control volume, the volume fractions of all phases sum to unity. The fields for all variables and properties are shared by the phases and represent volume-averaged values, as long as the volume fraction of each of the phases is known at each location. Thus the variables and properties in any given cell are either purely representative of one of the phases, or representative of a mixture of the phases, depending upon the volume fraction values. In other words the q th fluid's volume fraction in the cell is denoted as α_q , and then the following three conditions are possible:

$\alpha_q = 0$: the cell is empty (of the q th fluid)

$\alpha_q = 1$: the cell is full (of the q th fluid)

$0 < \alpha_q < 1$: the cell contains interface between the q th fluid and one or more other fluids.

4.1.1 The Volume Fraction Equation

In the VOF model, the volume fraction of water, α_w , is calculated by the following continuity equation:

$$\frac{\partial \alpha_w}{\partial t} + \mathbf{v} \cdot \nabla \alpha_w = 0, \quad (4.1)$$

Where \mathbf{v} is the velocity vector. By its definition, the volume fraction of air, α_a , is

$$\alpha_a = 1 - \alpha_w. \quad (4.2)$$

Density ρ and viscosity μ of the fluid are respectively calculated using the volume fraction of water:

$$\rho = \alpha_w \rho_w + (1 - \alpha_w) \rho_a, \quad (4.3)$$

$$\mu = \alpha_w \mu_w + (1 - \alpha_w) \mu_a, \quad (4.4)$$

Where subscripts w and a respectively denote water and air.

4.1.2 The Momentum Equation

A single momentum conservation equation is solved throughout the computational domain, and the resulting velocity field is shared among the phases. However, the momentum equation, shown below, is dependent on the volume fractions through Eqs. 4.3 and 4.4.

$$\frac{\partial}{\partial t}(\rho \mathbf{v}) + \nabla \cdot (\rho \mathbf{v} \mathbf{v}) = -\nabla p + \nabla \cdot [\mu(\nabla \mathbf{v} + \nabla \mathbf{v}^T)] + \rho \mathbf{g}. \quad (4.5)$$

To simplify the problem, the following simple initial conditions are given for the initial water velocity components

$$v_r = v_z = 0, \quad v_\theta = \Omega r, \quad (4.6)$$

Where Ω is the angular velocity and is an arbitrary parameter that shows the strength of initial tangential motion in the ladle.

4.2 RESULTS OF NUMERICAL SIMULATION

4.2.1 Temporal Behavior of water surface

Two typical histories ($\Omega = 0.5$ and 1.5 1/s, small scale model) of the water surface location, predicted by our CFD model, are shown in Figures. 4.1 and 4.2. In these figures, the water surface is defined by $\alpha_w = 0.5$. Our CFD model successfully captured the vortex formation in the ladle. It can be seen from the figures that larger initial tangential velocity (i.e. larger Ω) causes higher critical height. It should be noted that the vortex depth fluctuates with time in Fig. 4.1, probably because of a hydrodynamic instability.

4.2.2 Velocity Flow fields

Figure 4.3 shows the predicted velocity fields at different instances for the small scale model at $\Omega = 1.5$ 1/s. Note that only one half section of the cylinder side view is shown. From Figure 4.2, it is clear that at $t = 10$ sec, there is no vortex formation and the corresponding flow field shows that the surface of the liquid level does not contribute to the drainage through the nozzle, i.e. only tangential velocities exist at the surface although there is draw down of the liquid through the nozzle. Thus, there is no entrainment of the top surface of the liquid level in the absence of a vortex. At $t = 20$ sec, a vortex starts to form at the surface and the velocity fields at the surface start to move axially downward. The tangential velocities are transformed into downward axial velocities via movement in radial direction due to the formation of a vortex.

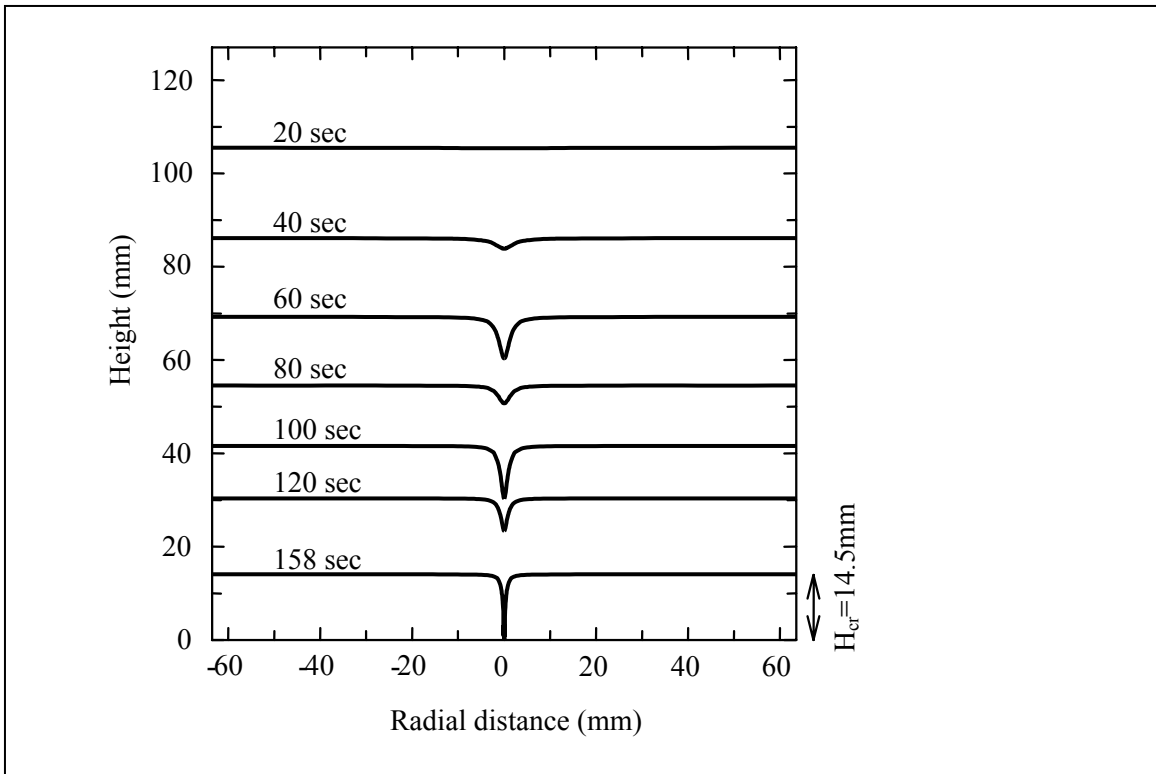


Figure 4.1: History of water surface location ($\Omega = 0.5$ 1/s)

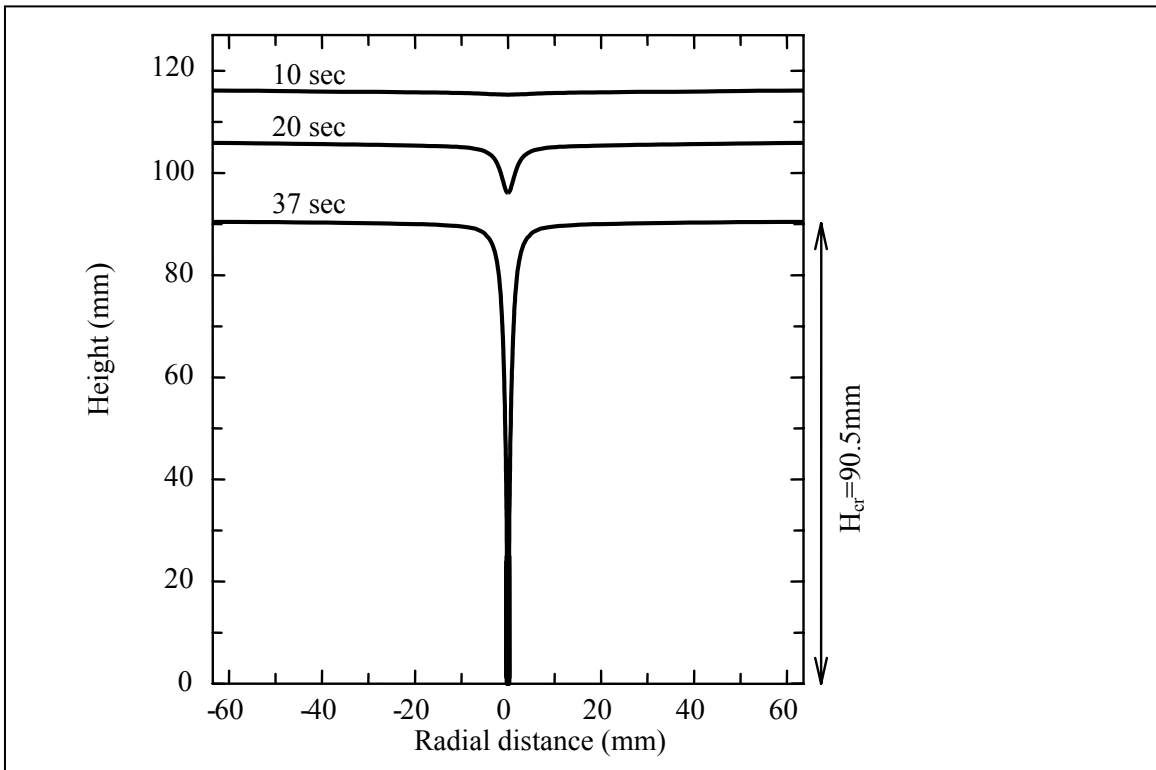


Figure 4.2: History of water surface location ($\Omega = 1.5$ 1/s)

During this change, the radial velocities that are formed due to vortex motion aid in the movement of the top surface (floating slag in case of steelmaking ladle), which was until now merely rotating on the surface into the core of the vortex. Near the core of the vortex, the local tangential velocities are high which further increase the radial velocities and this synergistic interaction between the radial and tangential velocities at the core creates high downward axial velocities and thus entrainment through the core. At $t=37$ sec, the vortex is fully developed and reached the bottom of the nozzle. At this instant there are high velocity fields and thus more amount of entrainment through the nozzle.

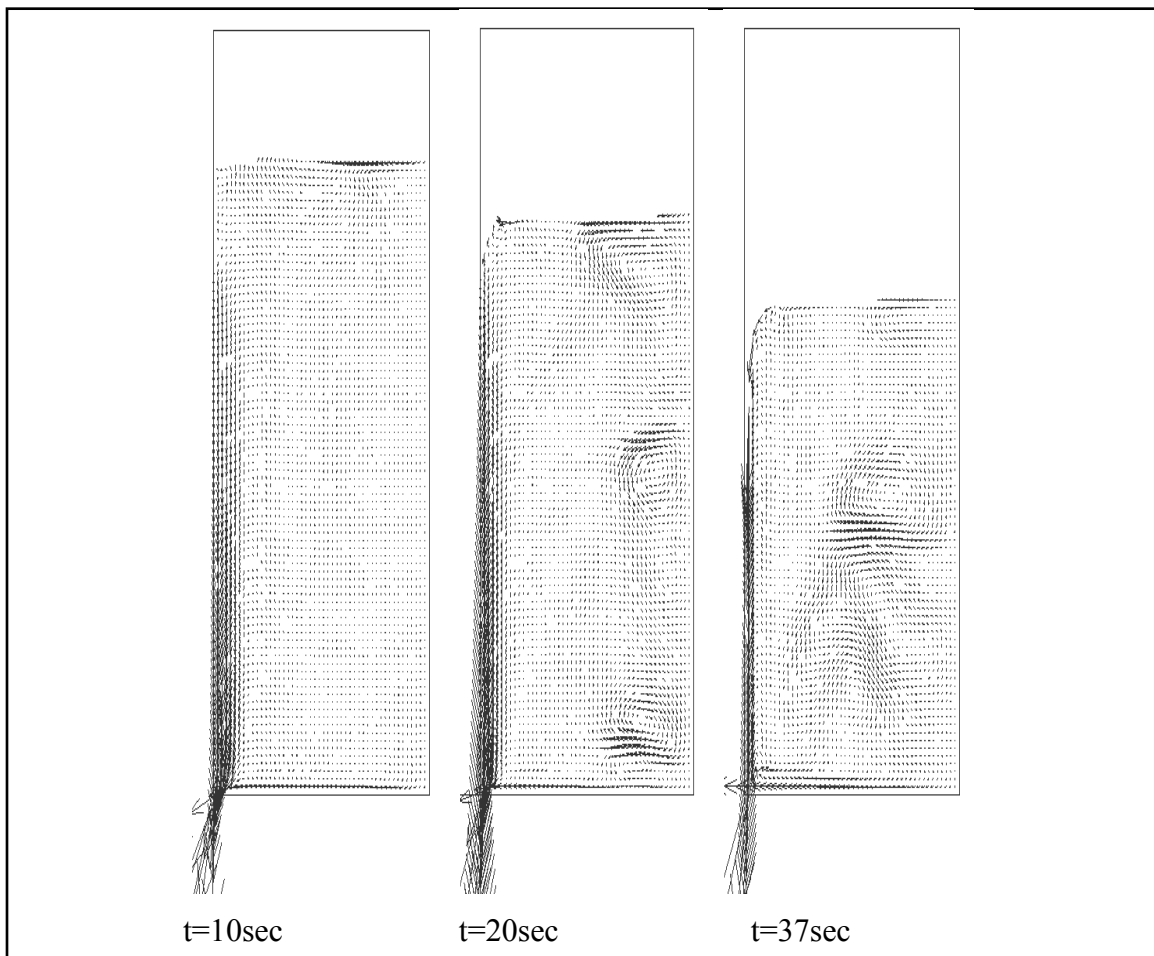


Figure 4.3: Predicted velocity fields ($\Omega = 1.5$ 1/s)

CHAPTER 5

SCALE MODELING ANALYSIS

4.1 INTRODUCTION

In this chapter, a physical analysis of the teeming process with vortex formation will be presented by forming dimensionless numbers that are relevant to the process. For this purpose, the pi-number method [21] has been employed. The pi-number approach involves the formulation of non-dimensional pi-numbers using the governing equations. A pi-number typically shows a relationship between two governing forces. A number of pi-numbers can be constituted depending on the assumed governing equations and then with the help of experimental results, the relative importance of these pi-numbers in the process can be studied. Since onsite measurements on the prototype would be impractical, the verification of experimental data obtained from a single model can be achieved by performing the same experiments on another scale (half scale in the present study). In addition, the results obtained from numerical simulations can be verified from the model experimental results. The aim of the scaling analysis is thus not only to formulate and verify the governing equations but also confirm results obtained from other methods.

4.2 SCALING LAWS FORMULATION

Since teeming is a gravity driven process involving rotating mass of molten steel, it is assumed that it is governed by the gravitational, inertial and viscous forces. Using these forces, three governing equations can be thus formulated:

$$\begin{aligned} F_g &= \text{mass} \times \text{acceleration} \\ \text{Gravitational Force:} &= m \times g \\ &= V \times \rho \times g \end{aligned}$$

$$\begin{aligned} F_i &= \text{mass} \times \text{acceleration} \\ \text{Inertial Force:} &= m \times a \\ &= V \times \rho \times a \end{aligned}$$

$$\begin{aligned} F_v &= \text{viscous shear strength} \times \text{area} \\ \text{Viscous Force:} &= \tau \times A \end{aligned}$$

These three governing forces yield to two pi-numbers:

$$\pi_1 = Re = \frac{\text{Inertial Force}}{\text{Viscous Force}} = \frac{F_i}{F_v} = \frac{V \times \rho \times a}{\tau \times A}$$

$$= \frac{\rho \times D \times V}{\mu} = \frac{D \times V}{\nu}$$

Where V = Volume of water

ρ = Density of water

D = Diameter of cylinder

μ = Dynamic Viscosity of water

ν = Kinematic Viscosity of water ($= \mu / D$).

Re equality between the two scale models implies:

$$\frac{D_1 \times V_1}{\nu_1} = \frac{D_2 \times V_2}{\nu_2}$$

Where the subscripts 1 and 2 represent the big and small models. Since the kinematic viscosity of molten steel is almost the same as that of water (approximately $1\text{mm}^2/\text{sec}$), and water being used for both the scale model experiments, $\nu_1 = \nu_2$ and since the big model is twice in diameter to the small model, $D_1 = 2D_2$. The final relationship between velocities is thus:

$$V_2 = 2V_1 \quad (5.1)$$

i.e. for same Re , the small model must have twice the initial tangential velocity as the big model.

In a similar manner, the second pi-number is derived as

$$\pi_2 = Fr = \frac{\text{Inertial Force}}{\text{Gravitational Force}} = \frac{F_i}{F_g} = \frac{V \times \rho \times a}{m \times g}$$

$$= \frac{V}{\sqrt{gD}}$$

Froude number equality for the two models implies:

$$\frac{V_1}{\sqrt{gD_1}} = \frac{V_2}{\sqrt{gD_2}}$$

$$\text{Or } V_1 = \sqrt{2} V_2 \quad (5.2)$$

i.e for same Fr , the big model must have initial tangential velocity that is $\sqrt{2}$ times faster than that in the small model. Thus, it is clear from Eqs. (5.1) and (5.2) that it would be impossible to satisfy Re and Fr equalities simultaneously.

The objective of the scale model experiments is thus to provide a deeper insight into the vortex formation phenomenon by studying the relative significance of the non-dimensional numbers Re and Fr on the teeming process with vortex formation. An attempt will be made to highlight the governing factors and the scale modeling considerations that would be helpful in the overall goal of prevention of slag entrainment during the steel teeming process.

CHAPTER 6

RESULTS AND DISCUSSIONS

6.1 INTRODUCTION

In this chapter, several results obtained from the experimental procedures are presented. The same sets of experiments were performed on both the scale models (represented as big and small models). In the first set of experiments, the laser beam was shot at the cylinder in a horizontal direction. The CCD camera was focused on the top surface of the water in the cylinder such that the initial tangential velocity could then be captured by the data acquisition system. A video camera was placed alongside the cylinder so that the events occurring since the opening of the nozzle to the end of drainage were recorded and studied. Also, the several images obtained from the video were used to decide the critical height (the height of water level at the instant the vortex reaches the bottom of the cylinder). Several experiments were then performed in a similar manner with varying initial tangential velocities. It should be noted that although the value of initial tangential velocity could not be predetermined in a run, a number of runs with different stirring speeds (rotational motion imparted to water to obtain tangential velocity flow) and different holding times (time between end of stirring and beginning of nozzle drainage) were maintained to make sure that a range of critical heights were achieved, i.e. the onset of vortex ranged from very quick to very slow. The value of the initial tangential velocity could be determined after the completion of a single run by the data acquisition system. In this manner, the two major quantities of interest, i.e. the initial tangential velocity and the critical heights were determined and analyzed further.

6.2 CHARACTERISTICS OF TANGENTIAL VELOCITY

It is now established that the initial tangential velocity imparted to the water during the filling of the cylinder is responsible for the creation of vortex. To study the characteristics of this tangential velocity, the tangential velocity at different radial positions from the centre of the cylinder was measured using the PIV data acquisition system for the big scale model. A high initial tangential velocity was imparted to the water before the measurements were made in order to make sure that a vortex would form in due course of the experiment. Thus the measurements correspond to the vortex formation velocity measurements. Figure 6.1 shows the variation of tangential velocity in the radial direction. The tangential velocity increases linearly from the centre of the cylinder till the core radius is reached after which it decreases inversely with the

radius. Thus the tangential velocity follows a Rankine type vortex in which the velocity is defined as

$$V_{\theta} = \omega r \quad 0 \leq r \leq a$$

$$V_{\theta} = \frac{\omega a^2}{r} \quad r \geq a$$

Here a is the core radius of the vortex, ω is the angular velocity at radius r . The characteristic initial tangential velocity, $V_{\theta,i}$, is defined by

$$V_{\theta,i} = \Omega R,$$

Where Ω is the angular velocity at radius R .

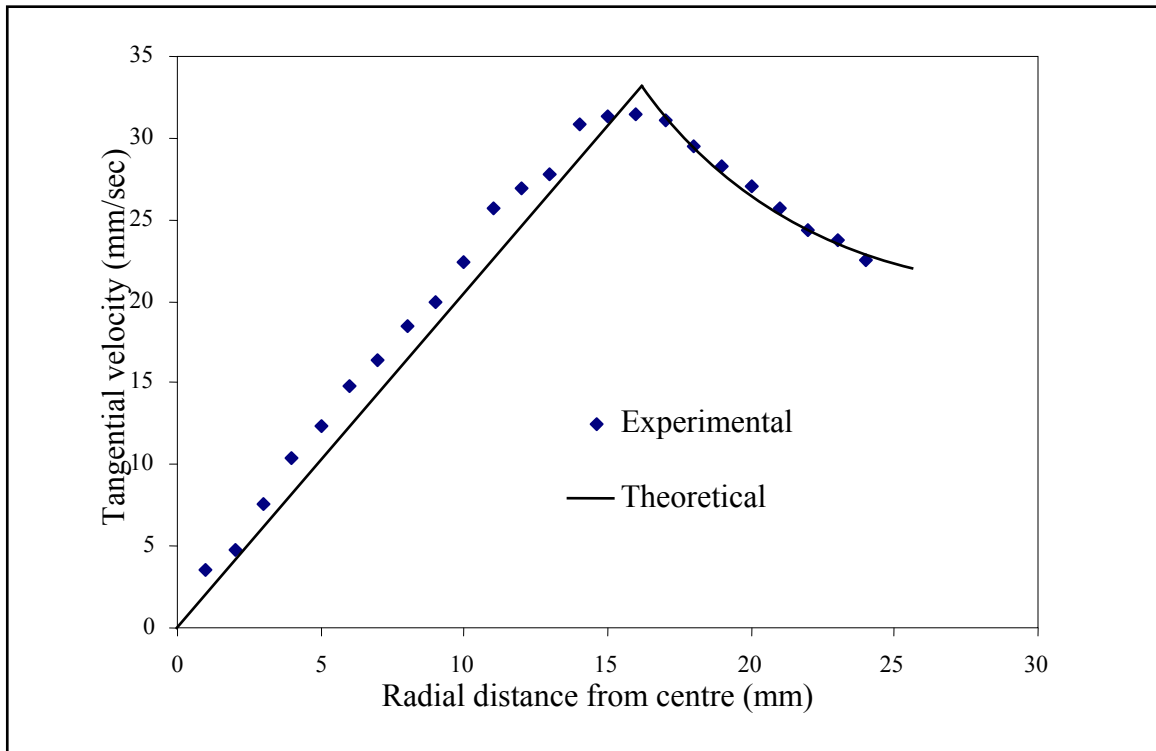


Figure 6.1: Variation of tangential velocity along the radius

6.3 VARIATION OF CRITICAL HEIGHTS WITH VARYING INITIAL TANGENTIAL VELOCITIES

The values of critical heights obtained for the two scale models were plotted against the corresponding Initial tangential velocities. The plot shows the importance of the role played by initial tangential velocities in the vortex formation phenomenon.

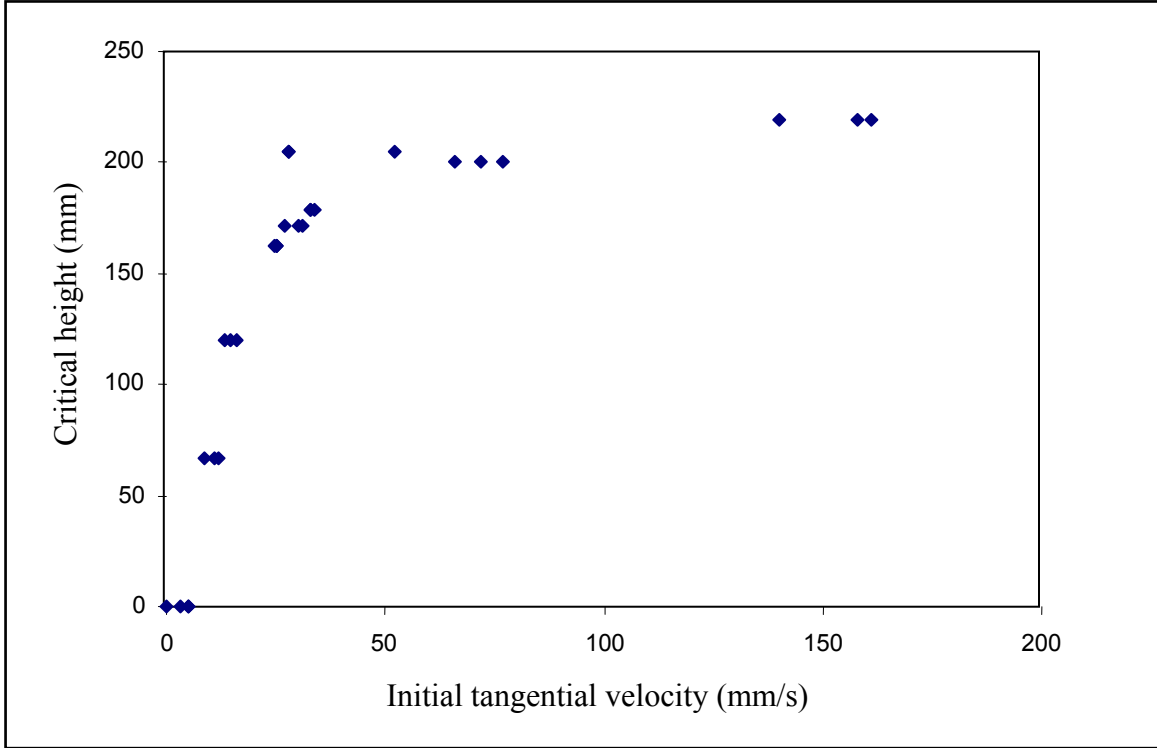


Figure 6.2: Critical height vs. initial tangential velocity (big model)

Figure 6.2 shows the variation of critical height, H_{cr} , with $V_{\theta,i}$ for the big scale model. The plot can be divided into three distinct regions which are described below.

- (a) At low initial tangential velocities, less than approximately 10 mm/s, H_{cr} is nearly zero and independent of $V_{\theta,i}$ (non-vortexing funnel regime), confirming that the initial tangential velocity is responsible for the vortex formation.
- (b) As $V_{\theta,i}$ increases from 10 to 30 mm/s, H_{cr} increases rapidly to reach about 40-50 % of the initial liquid height, H_0 . This is the vortexing region in which there is a linear increase in H_{cr} with $V_{\theta,i}$.
- (c) With further increase in $V_{\theta,i}$ (> 30 mm/s), H_{cr} slowly increases, asymptoting to the initial liquid height, H_0 .

A similar plot was obtained for the small scale model (Figure 6.3) validating the scale model experiments and confirming the scalability of the teeming process with vortex formation. The experimental results were compared with the results obtained from numerical simulation using VOF model. Figure 6.4 shows the combined plot of initial tangential velocity vs. critical height for both scale models obtained from scale model experiments and numerical simulations.

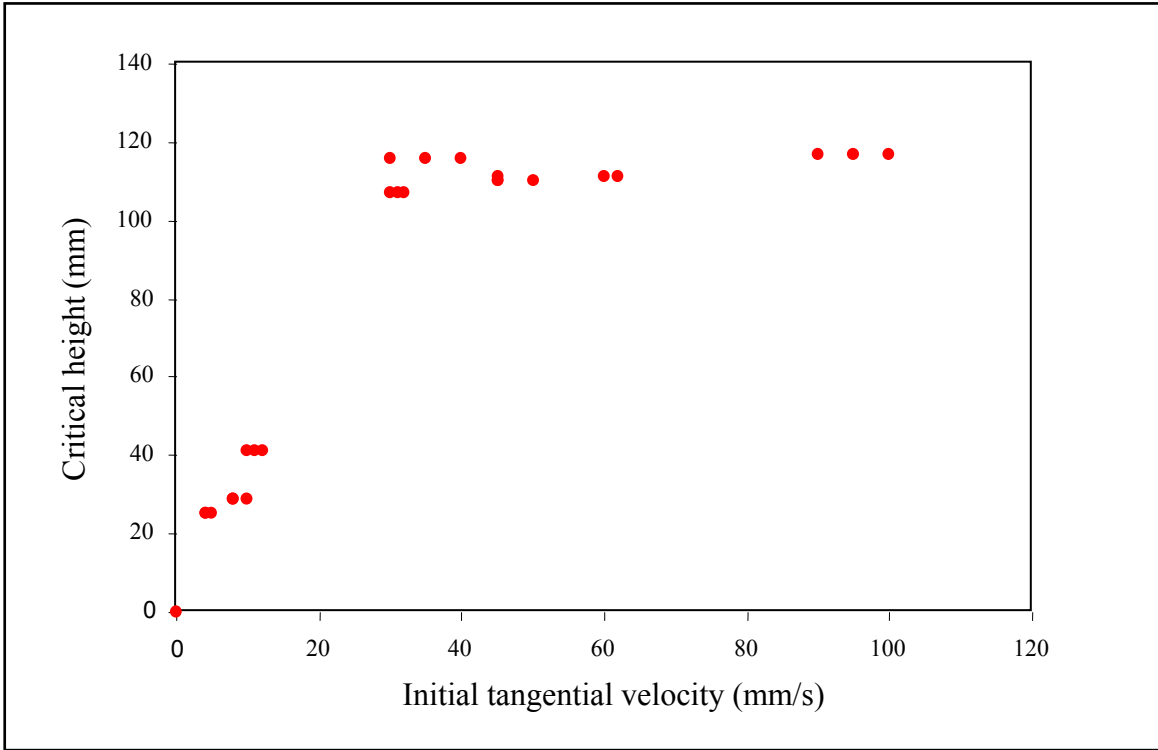


Figure 6.3: Critical height vs. initial tangential velocity (small model)

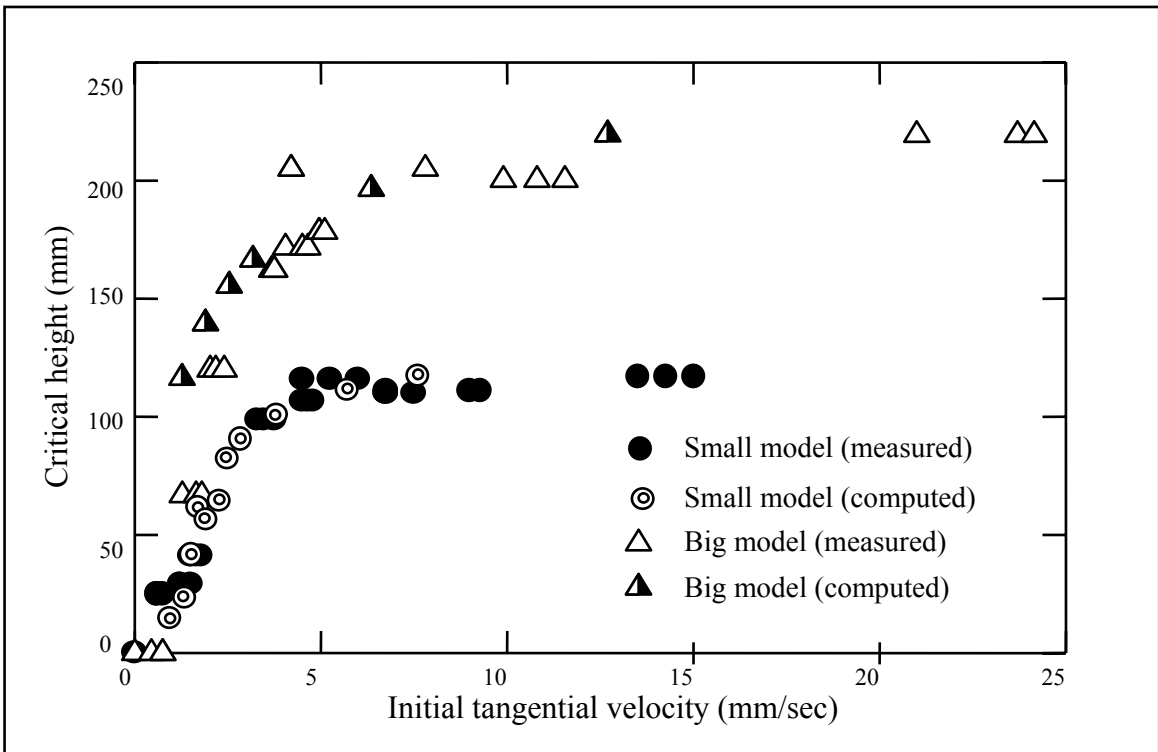


Figure 6.4: Comparison of experimental and numerical results

The experimental values are in good agreement with the numerical values obtained from the VOF model in both the scales, confirming that the VOF model can successfully capture the critical height of vortex formation in the steel teeming process.

6.4 NON-DIMENSIONAL PLOTS OF INITIAL TANGENTIAL VELOCITY VS. CRITICAL HEIGHT

The above plot of initial tangential velocity vs. critical height was non-dimensionalised by dividing the critical height (H_{cr}) with the initial height of water in the cylinder (H_i). The initial height of water level was chosen to non-dimensionalize H_{cr} , instead of any other fixed dimension of the cylinder (e.g. diameter) because in addition to being a constant for a single scale model, H_{cr}/H_i would explain the height of the vortex in relation to the initial height of water, i.e it would be a measure of the time taken for vortex formation soon after drainage begins. Note that the value of H_{cr}/H_i ranges from 0 to 1 but can never exceed unity as the vortex can at best form immediately after drainage begins and at worst at the far end of the drainage process.

The initial tangential velocity was non-dimensionalised into two dimensionless numbers, i.e. Reynolds number (Re) and Froude Number (Fr). The reason for choosing these two dimensionless numbers is the assumption that the steel teeming process is governed by three major forces: inertial force (F_i), gravitational force (F_g) and viscous force (F_v). Other forces such as the surface tension force were neglected on the basis that it would be negligible compared to the dominant forces of inertia, gravity and viscosity. Also, surface tension reduces with increased temperatures and since molten steel in the ladle is at temperatures in excess of 600°C, it is reasonable to assume that surface tension forces play a negligible role in vortex formation. Also, no temperature effects were considered during scaling analysis although the molten steel poured in the ladle is at such high temperatures whereas water at room temperature was used in the experiments. This is based on the reasoning that although there are high temperatures inside the ladle, there is no vertical or horizontal temperature gradient, i.e. the molten steel temperature is uniform throughout the ladle largely due to the refractory coatings that maintain a constant temperature inside without heat losses. Hence, the net effect of high temperatures is negligible and need not be considered in the analysis. Other forces such as the Coriolis force (the effect of earth's rotation) were neglected as they are dominant in cases where the sizes are comparable to earth's diameter.

On the basis of these assumptions, the initial tangential velocity was non-dimensionalised using the pi-number approach of scale modeling into Re and Fr and was plotted against the non-dimensional critical height as discussed below.

6.4.1 Variation of Non-Dimensional Critical Height (H_{cr} / H_i) with Reynolds Number (Re)

The Reynolds number is calculated from the initial tangential velocity as follows:

$$Re = \frac{\text{Inertialforce}}{\text{ViscousForce}} = \frac{V_{\theta,i} \times D}{\nu}$$

Where D = Diameter of the cylinder

ν = Kinematic viscosity of water, and

$V_{\theta,i}$ = Initial tangential velocity of water.

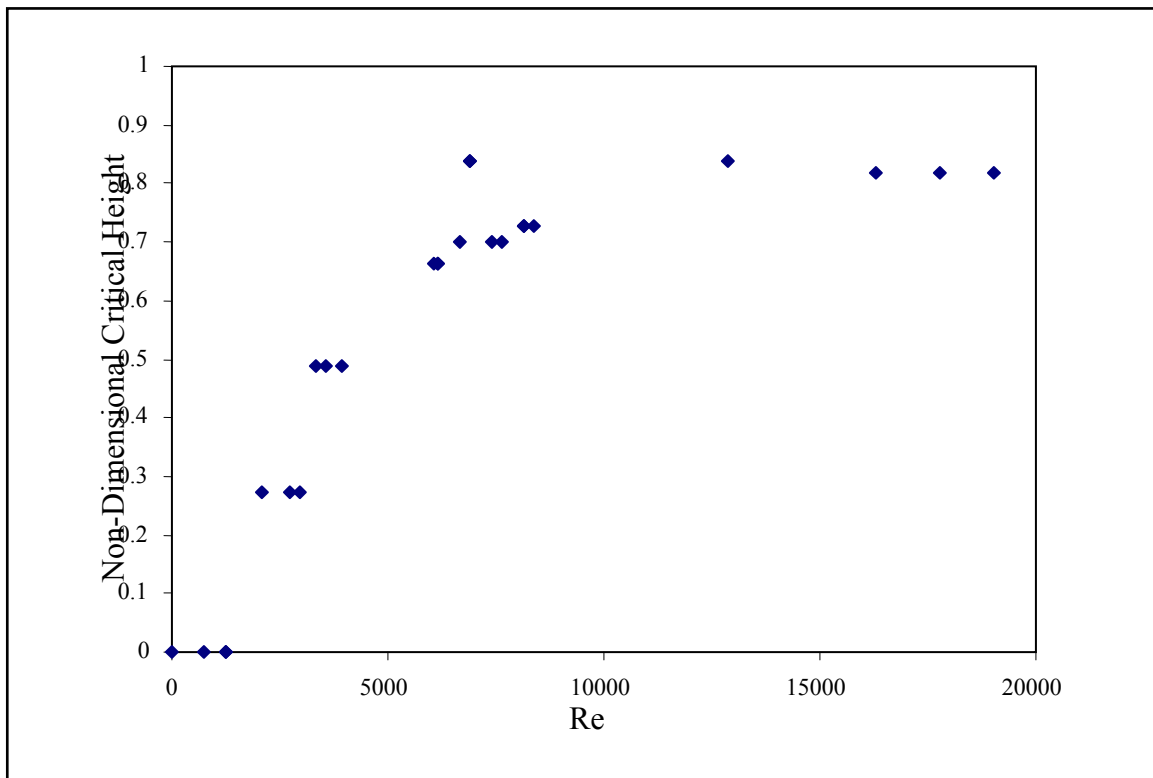


Figure 6.5: Non-Dimensional Critical Height vs. Reynolds Number (Big Model)

A similar trend is observed for both the scale models as is seen from Figures. 6.5 and 6.6. The high values of Re on the horizontal axes in the vortexing region suggests that vortex formation occurs at turbulent flows with Re exceeding 2000 (inertial forces dominate over the viscous forces). Also, the trend is quite similar to the dimensional plot of $V_{\theta,i}$ vs. H_{cr} for both the scale models (this is understandable from the fact that the H_{cr} / H_i vs. Re plot is obtained from

the $V_{\theta,i}$ vs. H_{cr} plot quite simply by dividing both quantities with constant values, ν/D and H_i respectively. Note that in the vortexing region, the values of Re for both the scale models extend upto 10,000 but the corresponding H_{cr} / H_i values differ slightly. The big model has a maximum value of H_{cr} / H_i around 0.8 whereas the small one has H_{cr} / H_i around 0.9.

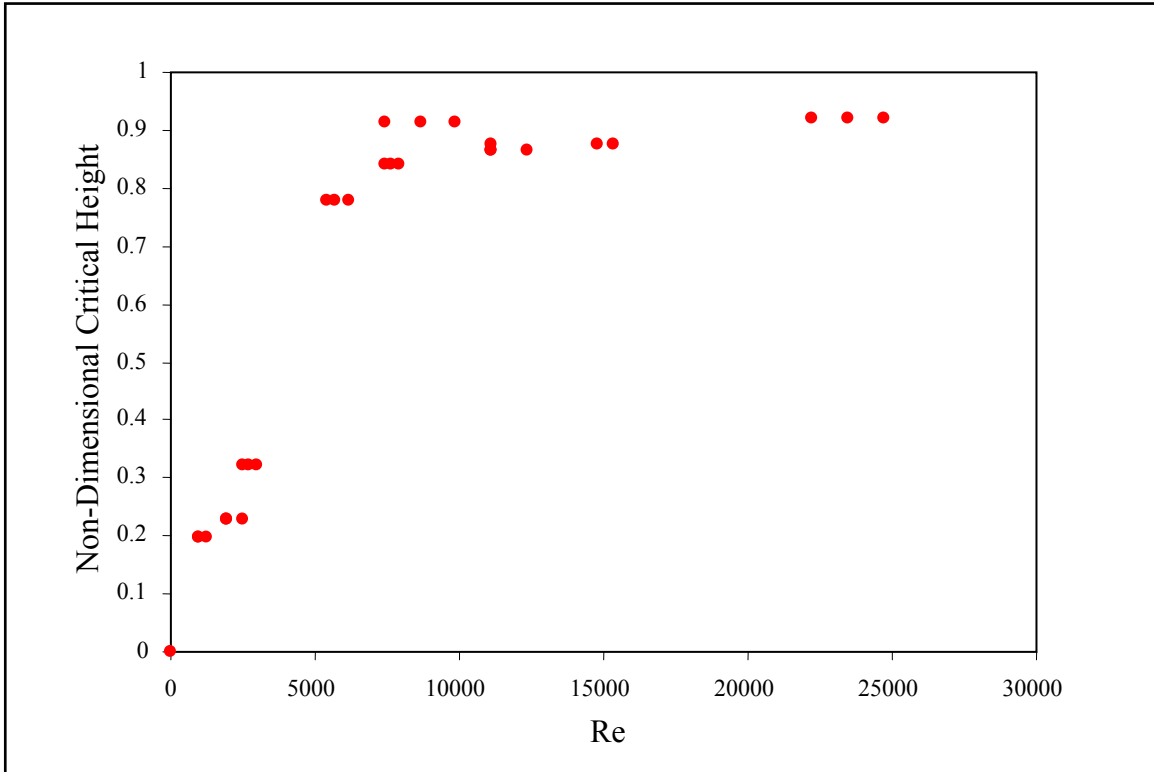


Figure 6.6: Non-Dimensional Critical Height vs. Reynolds Number (Small Model)

Comparison of H_{cr} / H_i vs. Re for the two Scale Models

Figure 6.7 shows the combined plot of H_{cr} / H_i vs. Re for the big and small scale models. It is evident from the plots that the trend lines for the two models are differing and there is less agreement between the two scales. For instance, at $Re = 5000$, the H_{cr} / H_i value for the Big model is around 0.6 whereas for the small model it is around 0.9 (note that both these values are in the corresponding vortexing regions which is the point of interest). Hence, for different scale models, the H_{cr} / H_i value for a fixed Re would be different, i.e. each scale model would

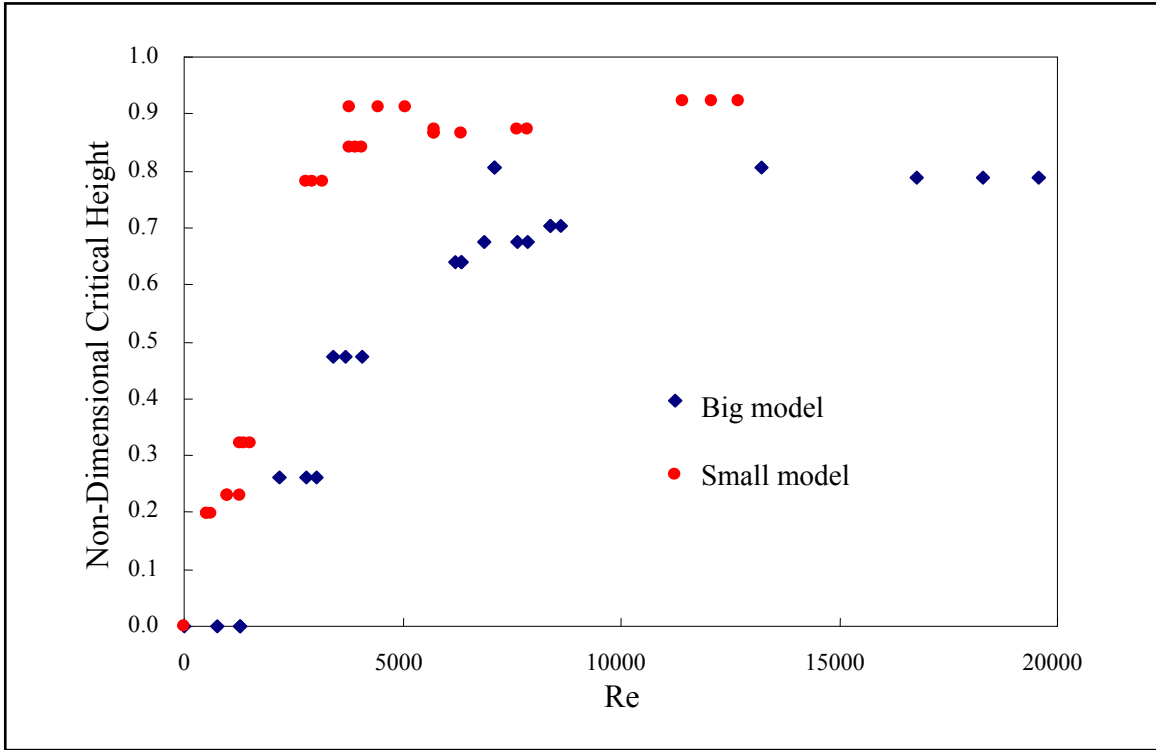


Figure 6.7: Comparison of non-Dimensional Critical Height vs. Reynolds Number

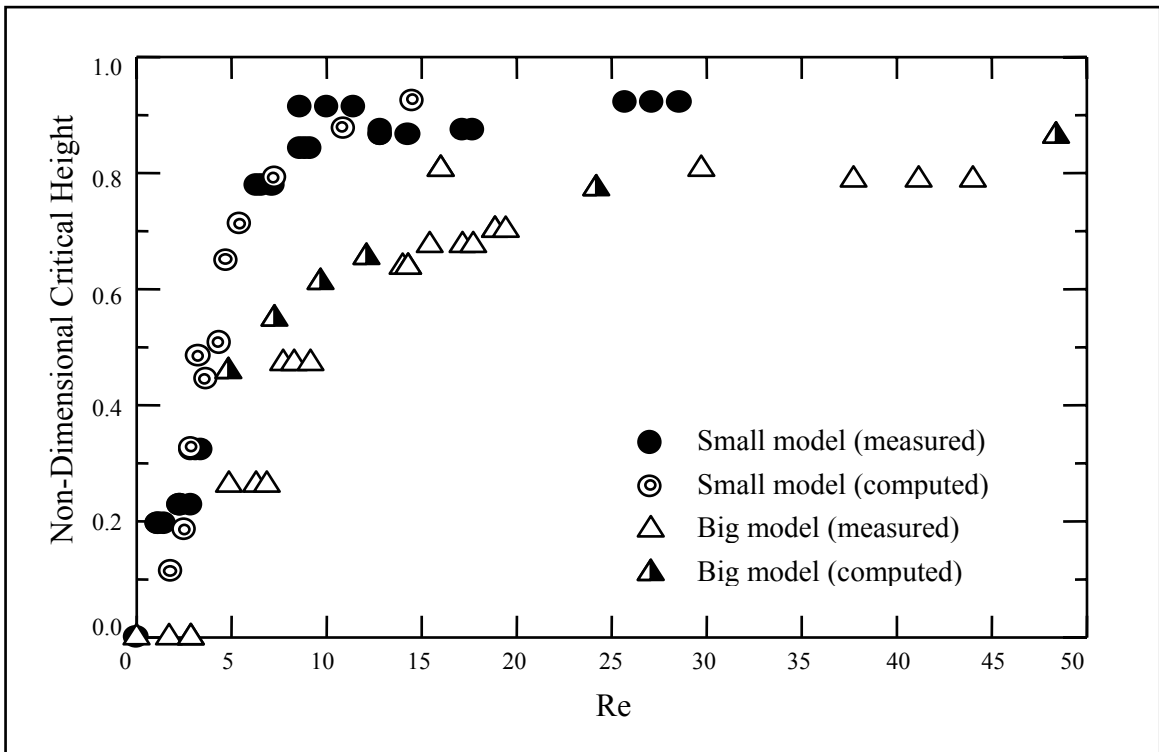


Figure 6.8: Comparison of experimental and numerical results

would have a different value of H_{cr} / H_i and it would be insufficient to predict the critical height of vortex formation in a prototype. The behavior of a prototype (steel making ladle) cannot be accurately studied for vortex formation using Re based modeling. Figure 6.8 shows the comparison between numerical and experimental results. These results further confirm the validity of the numerical VOF model.

6.4.2 Variation of Non-Dimensional Critical Height (H_{cr} / H_i) with Froude Number (Fr)

The Froude number is calculated from the initial tangential velocity as follows:

$$Re = \frac{\text{Inertial Force}}{\text{Gravitational Force}} = \frac{V_{\theta,i}}{\sqrt{g \times D}}$$

Where D = Diameter of the cylinder

g = Acceleration due to gravity

$V_{\theta,i}$ = Initial tangential velocity of water.

Again a similar trend is observed in case of both the scale models as shown in Figures 6.9 and 6.10. These plots are also similar in shape to the $V_{\theta,i}$ vs. H_{cr} plots owing to the fact that Froude number is obtained by dividing the $V_{\theta,i}$ term by a constant ($\sqrt{g \times D}$). Note that the values of Fr for both models extend upto 0.03 in the vortexing region showing that the gravitational forces dominate the inertial forces. Also, the corresponding H_{cr} / H_i values match very well for both the scale models.

Comparison of H_{cr} / H_i vs. Fr for the two Scale Models

The combined plot for H_{cr} / H_i vs. Fr for both scale models is shown in Figure 6.11. There is far more agreement between the two scales when compared to the Re curves. For example, at Fr = 0.02, the H_{cr} / H_i value for both models is around 0.7. Hence, for different scales, the H_{cr} / H_i value for a fixed Fr would be a constant value and thus the non-dimensional critical height can be expressed as a single function of Froude number and can be used to predict the critical height of vortex formation of the prototype.

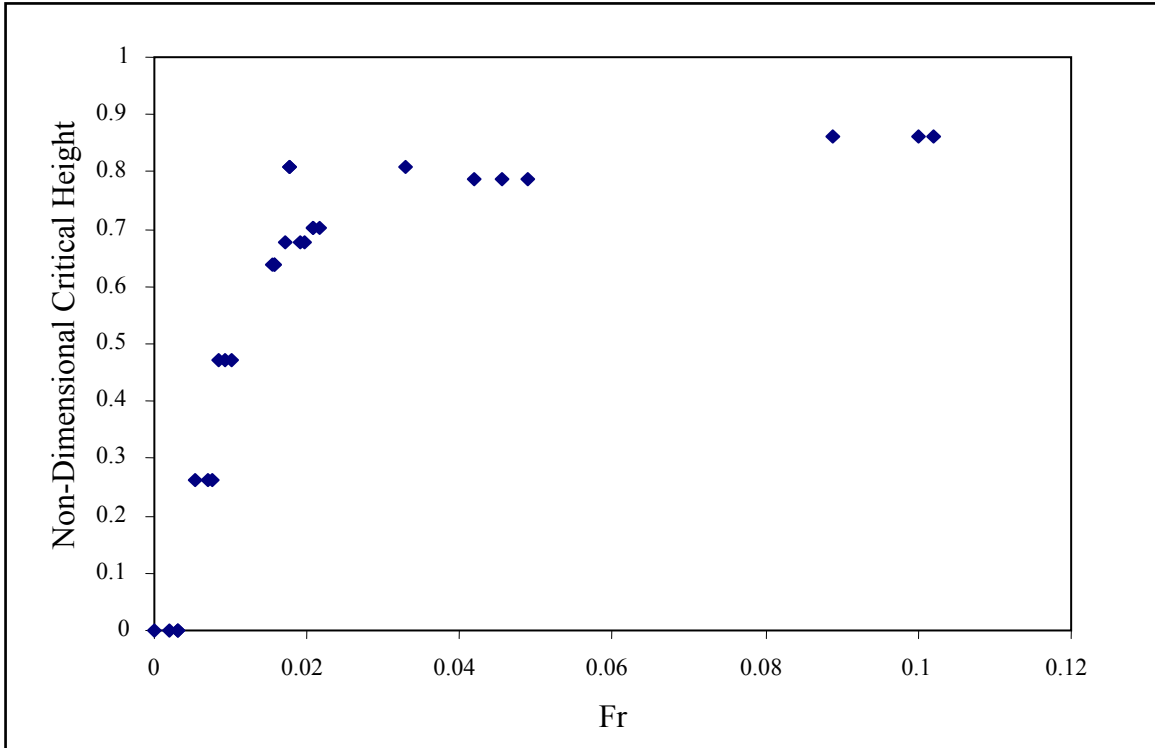


Figure 6.9: Non-Dimensional Critical Height vs. Froude Number (Big Model)

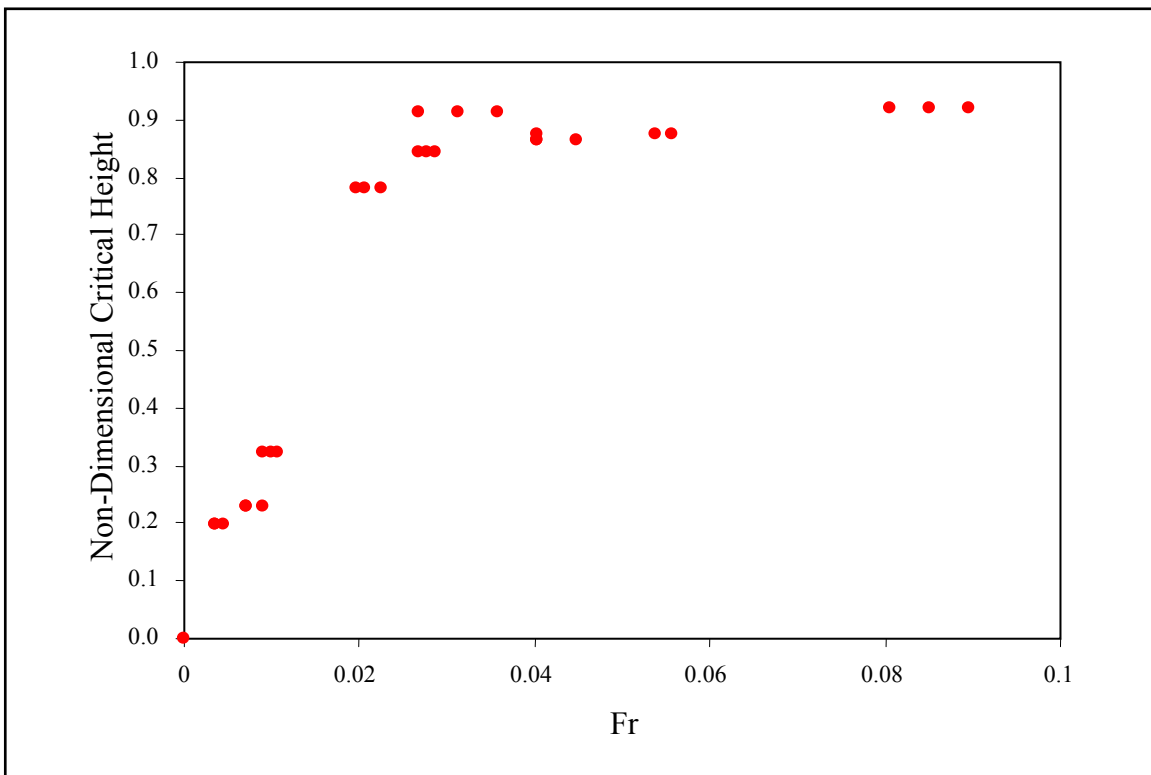


Figure 6.10: Non-Dimensional Critical Height vs. Froude Number (Small Model)

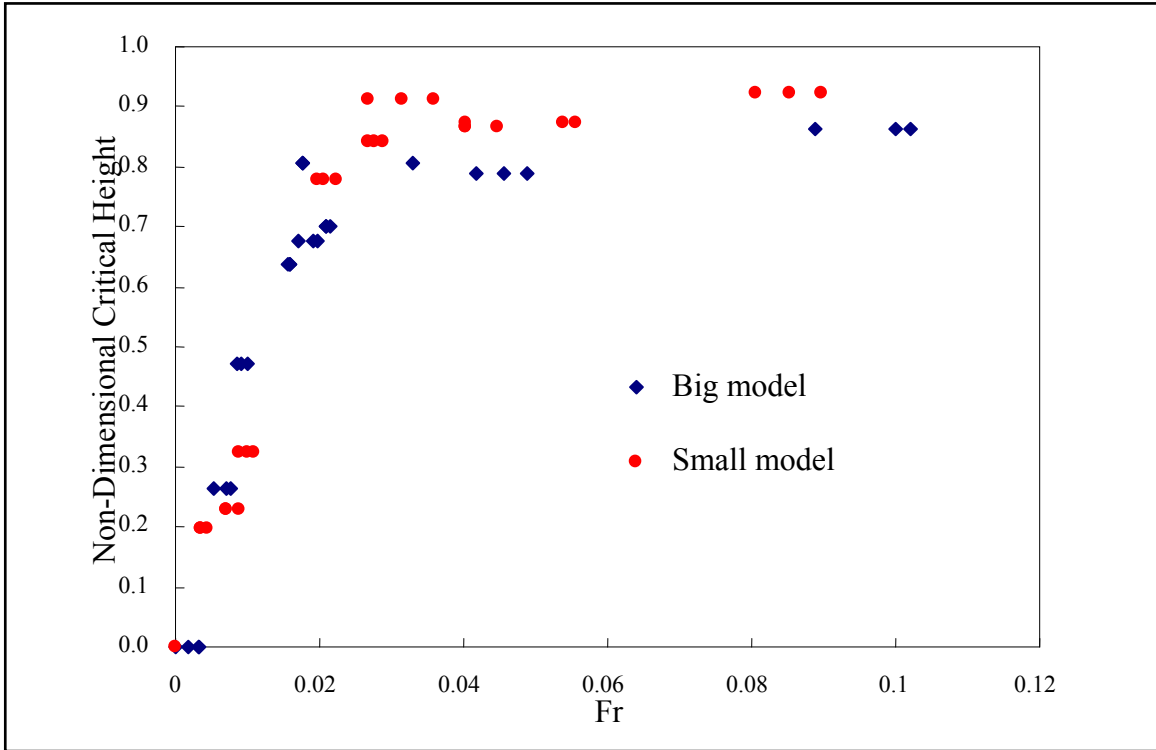


Figure 6.11: Comparison of non-Dimensional Critical Height vs. Froude Number

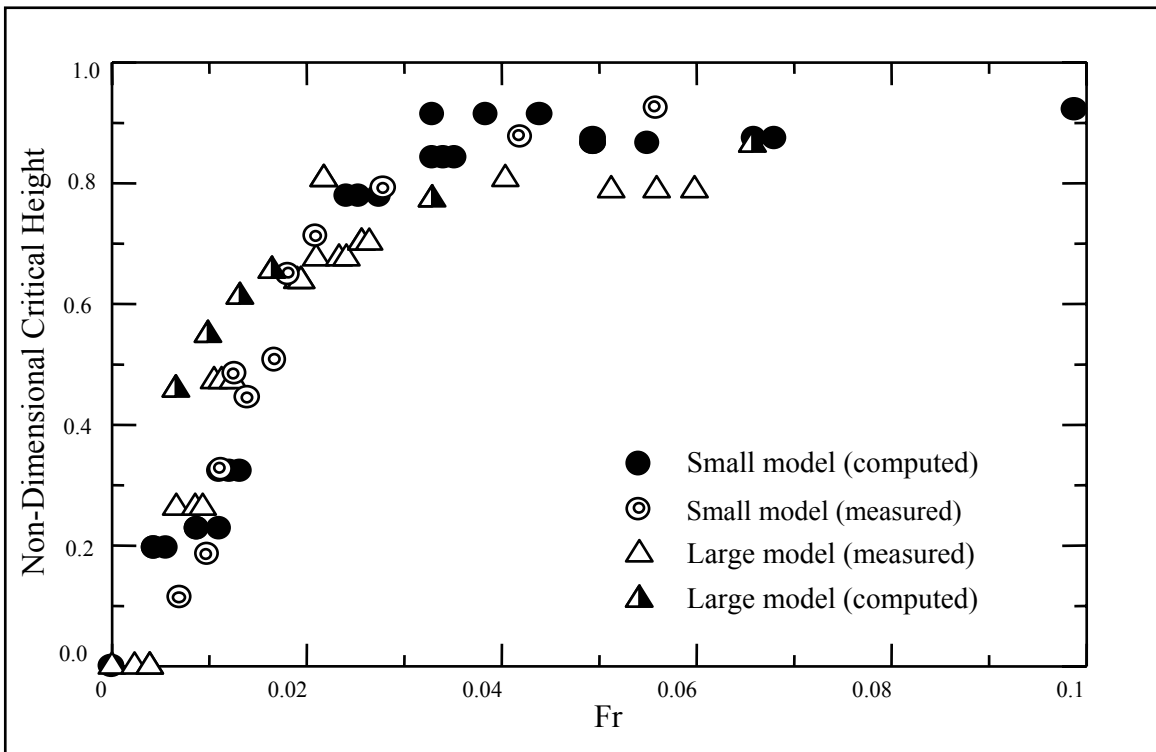


Figure 6.12: Comparison of experimental and numerical results

Figure 6.12 shows the combined plots for non-dimensional critical height vs. initial tangential velocity for both models obtained from experimental as well as numerical methods. The numerical simulations have good repeatability as can be seen from the plots for the two different scales. Further, they are in good agreement with the experimental results confirming the validity of the VOF model used in numerical simulations.

6.5 RELATIVE SIGNIFICANCE OF GOVERNING FORCES

To understand the relative importance of each governing force in the vortexing phenomenon, let us consider a data point on the H_{cr} / H_i vs. Re and H_{cr} / H_i vs. Fr plots (Figures 6.5 and 6.9). The point on the curve for the big scale model at which H_{cr} / H_i is 0.6383 is identified. The corresponding values of Re and Fr are

$$Re = 6350 \text{ and } Fr = 0.01584$$

$$\Leftrightarrow F_i = 6350 F_v \text{ and } F_i = 0.01584 F_g$$

$$\Leftrightarrow F_i > F_v \text{ and } F_g > F_i$$

$$\Leftrightarrow F_g > F_i > F_v$$

Thus the gravitational forces are most dominant in the teeming process followed by the inertial forces and then the viscous forces.

6.6 RELATION BETWEEN FROUDE NUMBER AND NON-DIMENSIONAL CRITICAL HEIGHT

It is clear from the H_{cr} / H_i vs. Fr plots that a single function can be used to express the Fr in terms of the H_{cr} / H_i . Figure 6.13 shows the plot for H_{cr} / H_i vs. Fr for the big scale model and a non-linear curve that fits all the data points was drawn. This non-linear function was found as the exponential associate distribution defined as

$$y = y_0 + A_1*(1 - \exp(-x/t_1)) + A_2*(1 - \exp(-x/t_2))$$

Here x refers to the Froude number and y refers to H_{cr} / H_i and y_0, A_1, A_2, t_1, t_2 are all constants.

6.7 RESULTS FOR EXPERIMENTS USING PIV WITH VERTICAL LASER BEAM

In this section, the results obtained from the experiments performed on the scale models using the Particle Image Velocitometry (PIV) technique with the laser beam striking the cylinder in a vertical plane are discussed. A qualitative analysis of the images and the corresponding vector profiles is presented. An explanation at illustrating the various stages of the vortex formation phenomenon using the velocity vector profiles has been made.

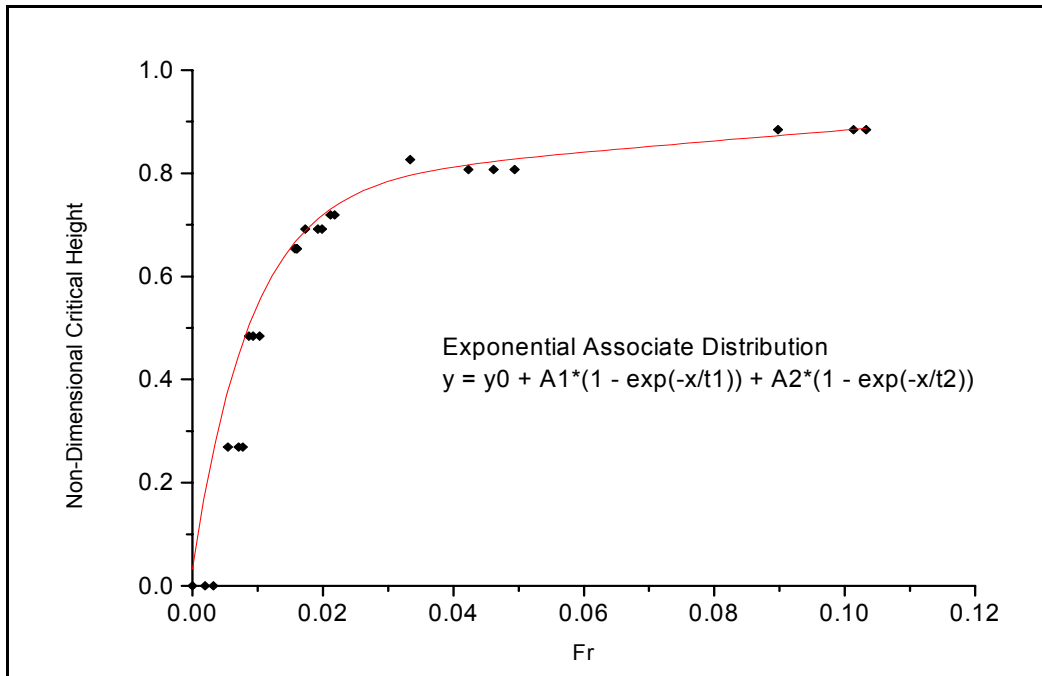


Figure 6.13: Curve fitting for the H_{cr} / H_i vs. Fr plot

This enabled the CCD camera to capture the top view and side view images and the corresponding velocity profiles at various stages in the vortex formation. It shows how the initial tangential velocity varies in direction and orientation at various stages. In particular, the side view images obtained enable the study of effects of radial and axial velocities in the vortex formation. Figure 6.14 shows the top view image obtained for the small scale model showing one half of the cylinder and the corresponding velocity profile obtained by PIV analysis. Note that in this case the initial tangential velocity is not strong enough to cause a vortex. The velocity profiles are perfectly tangential and there is no movement in the radial and axial directions. Figure 6.15 shows the side view image and velocity profile after a vortex starts appearing. The velocity profile validates the results obtained from numerical simulations (discussed in chapter 4). It clearly illustrates the transformation of the tangential velocities into radial and subsequent axial velocities (which are not clearly seen because of the scattering of seeding particles near the vortex core) in the presence of a vortex.

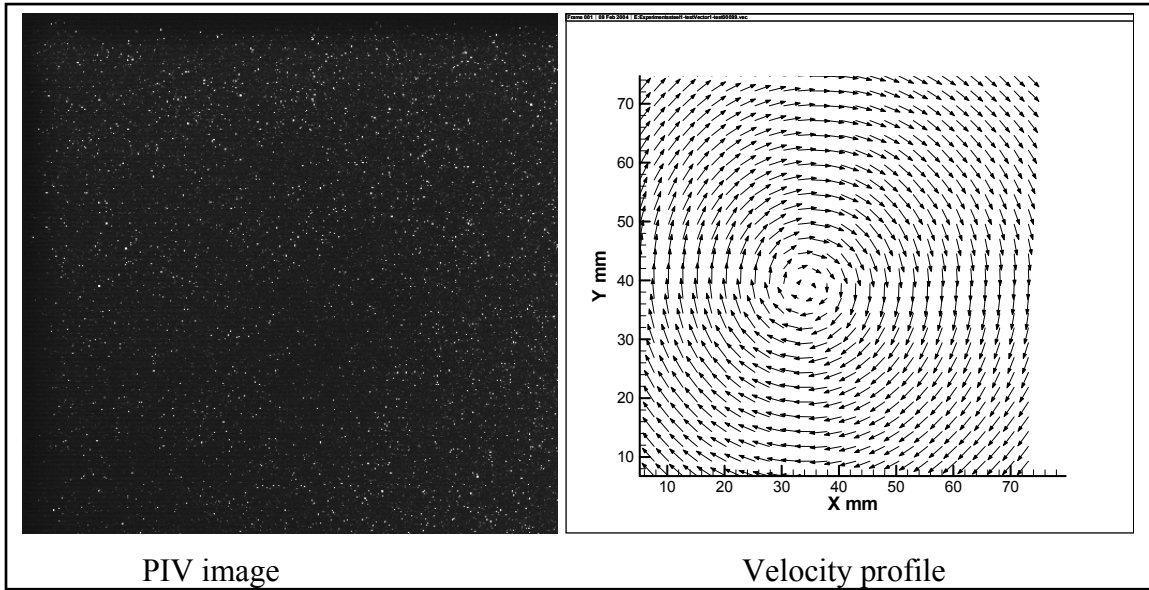


Figure 6.14: Top view PIV image and velocity profiles (no vortex)

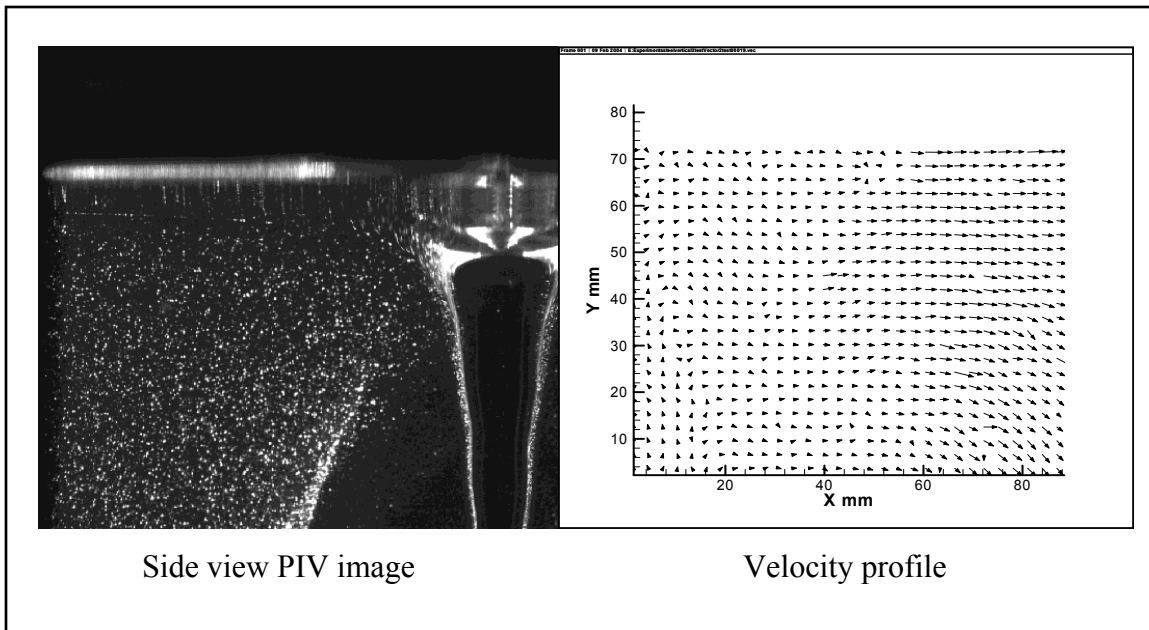


Figure 6.15: Side view of velocity profile (with vortex)

CHAPTER 7

SUMMARY AND CONCLUSIONS

7.1 INTRODUCTION

The minimization of slag entraining during the many liquid metal transfer operations involved in the continuous casting process is a primary concern of the steelmaking industry. Slag entrainment, and its minimization has a significant effect on the metal cleanliness, yield, and productivity of steel. Vortex formation is commonly considered to be one of the mechanisms for slag entrainment.

The objective of holding vessel drainage is to maximize the yield of the primary liquid, without entraining any supernatant phase. With the progressive emptying of a vessel, a situation frequently arises where the primary liquid loses the dynamics necessary to keep the drainage nozzle filled. When that happens, the supernatant fluid (be it a gas or a liquid) has to ‘fill-in’ for the inability of the primary liquid. The primary liquid can lose the dynamics necessary to keep the nozzle filled when the tangential velocity of the primary liquid along the central axis of the nozzle exceeds a critical value.

7.2 CONCLUDING REMARKS

Scale model experiments on teeming process were conducted on two scale models. The PIV technique was used to obtain the radial distributions of tangential velocity. The initial tangential velocity was found responsible for the vortex formation. The PIV system also enabled to study the effects of varying initial tangential velocities on the critical height of vortex formation. This was achieved by adopting the non-dimensional approach of scale modeling. Assumptions were made to simplify the teeming process with vortex formation and pi-numbers were derived as Reynolds number and Froude number from the governing equations. The experimental data enabled to investigate the dependence of teeming process on Reynolds and Froude numbers separately and Froude number was found to be the dominant pi-number. An expression for the relation between the critical height and Froude number was developed that can be used to predict the critical height of vortex formation of the prototype in terms of Froude number. The experimental results were validated by a numerical model. In addition, it was confirmed that the critical height can be numerically predicted using the VOF model. A deeper understanding of the vortex formation phenomenon was also achieved qualitatively with the help of the PIV images and velocity fields.

7.3 MODELING OF VORTEXING FUNNEL FORMATION

The relations determined from the present study may not be directly applicable to the estimation of critical height in actual steelmaking ladles, given that tangential velocity distributions therein are likely different from those studied. The difficulty lies in the uncertainty associated with the spatial and temporal distribution of tangential velocity in the ladle, the magnitude of these velocities themselves, and whether conditions favorable to vortexing funnel formation are prevalent.

In order for any such estimation to be possible, it will be necessary to track the temporal evolution of tangential velocity distributions in the vessel through various stages of liquid metal processing. Numerical techniques (as discussed in chapter 4) can be used to track the tangential velocity distribution in the ladle, both prior to and after the start of ladle teeming.

7.4 FUTURE WORK

The present study was concerned with the modeling of vortex formation during drainage of a ladle. In the present study it was assumed that the formation of a vortex would subsequently lead to the entrainment of slag floating on the surface of the liquid. Hence this study attempts to model the vortex formation phenomenon only and the slag flow was assumed to be similar to the behavior of air on the surface. Although this is a reasonable assumption, in actual ladle teeming process, the behavior of slag at high steel temperature needs to be accounted for. Forces such as surface tension may come into play that affects the movement of slag. The assumption that gravity, inertia and viscosity are the only dominant forces may need to be revised while considering actual prototype performance. At the end of this study, it can be stated that to model the vortex formation in teeming process, inertia and gravity are the major forces with viscosity playing a minor role. However, the need to model the slag flow during vortex formation is a separate issue and needs consideration of factors such as slag composition, viscosity of slag, slag reactions with molten steel at high temperatures etc. It is suggested that any future work in this field should account for these factors.

APPENDIX

NOMENCLATURE

A	Area of cross-section
a	Radial position, Acceleration
C_d	Discharge coefficient of drainage nozzle
D	Diameter of cylinder
D_1	Diameter of big cylinder
D_2	Diameter of small cylinder
d	Diameter of drainage nozzle
F_i	Inertial force
F_g	Gravitational force
F_v	Viscous force
Fr	Froude number
g	Acceleration due to gravity
H	Height of water
$H_{cr}, H_{cr,v}$	Critical height of vortex formation
h	Height of Rankine combined vortex's free surface at radius a with reference to the zero datum
h_o	Height of the lower tip of the Rankine combined vortex(at its axis) above the zero datum
K	Strength of vortex
m	Sink strength
p	Pressure
Re	Reynolds number
r	Radial coordinate
V_θ	Tangential velocity of water
$V_{\theta,i}$	Initial tangential velocity of water
α_q	Volume fraction of qth fluid in the cell
ω, Ω	Angular velocity
μ	Dynamic viscosity

ν	Kinematic viscosity
τ	Viscous shear strength
ϕ	Velocity potential
ψ	Stream function
θ	Angular position
ρ	Density
ζ	Vorticity
Γ	Circulation

REFERENCES

1. P. Hammersmid, K.-H. Tacke, H. Popper, L. Weber, M. Dubke and K. Schwerdtfeger, "Vortex formation during drainage of metallurgical vessels," *Iron and Steelmaking*, 11, No. 6, 1984, pp. 332-339
2. P. Andrzejewski, "Model Investigations of Slag Flow during Last Stages of Ladle Teeming," *Steel Research* 58, pp. 547-552 (1987)
3. D. R. F. Harleman, R. L. Morgan, R. A. Purple, "Selective Withdrawal from a Vertically Stratified Fluid," *Proceeding of the International Association for Hydraulic Research*, paper 10-c, pp. 1-16 (1959)
4. R. Sankaranarayanan and R. I. L. Guthrie, "Vortex Supression Device Improves Steel Cleanness," 14th PTD Conference Proceedings, pp. 87-99 (1995)
5. R. Sankaranarayanan and R. I. L. Guthrie, "Slag Entrainment through a 'Funnel' Vortex during Ladle Teeming Operations," *Proceedings of International Symposium on Development in Ladle Steelmaking and Continuous Casting*, pp. 66-87 (1990)
6. R. Sankaranarayanan and R. I. L. Guthrie, "A Laboratory Study of Slag Entrainment during Emptying of Metallurgical Vessels," *Steelmaking Conference Proceedings* 75, pp. 655-664 (1992)
7. E. Chang, "Review of Literature on Drain Vortices in Cylindrical Tanks," Report TN 1342, British Hydromechanics Research Association, 1976
8. R. I. L. Guthrie, "The Application of Transport Phenomenon to Ladle Steelmaking Operations," *Proceedings of McLean Symposium*, pp. 41-61 (1998)
9. R. I. L. Guthrie, "Fluid Flow in Metallurgy-Friend or Foe, " *Steelmaking Conference Proceedings* 83, pp. 511-543 (2000)
10. D. Mazumdar, " Fluid Flow, Particle Motion and Mixing in Ladle Metallurgy Operations," Ph.D. thesis, McGill University, Montreal, Canada (1985)
11. K. Hyounghae, "Physical Modeling of Two Phase Flows in Ladle-Shroud Systems," Masters thesis, McGill University, Montreal, Canada (1998)
12. H. H-Jewasinski and D. Sucker, "Stromungus- und Modelluntersuchungen zum Schlackemitlaufen aus Giebfannen mit Bodenausgub," *Stahl and Eisen*, 107, 1987, No. 23, pp. 1099-1104

13. D. Sucker, J.Reinecke and H. Hage-Jewasinski, *Stahl and Eisen*, 105, No. 14/15, 1985, pp. 765-769
14. R. Sankaranarayanan, “Modeling of Slag Entraining Funnel Formation (‘Vortex’) During Liquid Metal Transfer Operations,” Ph.D. thesis, McGill University, Montreal, Canada (1994)
15. A.W. Cramb and M. Byrne, “ Tundish slag entrainment at Bethlehem’s Burns Harbor (Indiana) Slab Caster,” *Steelmaking Conference Proceedings, ISS-AIME*, 67, 1984, pp. 5-13
16. D.J. Harris and J.D. Young, “Water Modeling- A variable Production Tool,” *Steelmaking Conference Proceedings, ISS-AIME*, 65, 1984, pp. 3-16
17. M.B. Dubke and K. Schwerdtfeger, “ Phenomena occurring during drainage of metallurgical vessels: Effect of stopper rod on vortex formation and development of surface waves,” *Ironmaking and Steelmaking*, 17, No.3, 1990, pp. 184-192
18. K. Schwerdtfeger, “ Fundamentals for Refining and Solidification Processing,” *Proceedings of the Sixth International Iron and Steel Congress, ISIJ, Nagoya, Japan, 1990*, pp.580-590
19. A.H. Shapiro, “ Vorticity,” in “*Illustrated Experiments in Fluid Mechanics*,” *The NCFMF Book of Film Notes, The MIT Press, Cambridge, Massachusetts, 1972,1988*, pp. 63-74
20. <http://www.tsi.com/fluid/products/> piv
21. R. I. Emori and D. J. Schuring, “*Scale Models in Engineering*,” Pergamon Press (1977)

VITA

Date and Place of Birth

- October 16, 1980 in Ahmednagar, Maharashtra, INDIA

Education

- Bachelor's Degree in Mechanical Engineering (B.E.), Chaitanya Bharathi Institute of Technology, affiliated to Osmania University, Hyderabad INDIA (2001)

Work Experience

- Worked as a Research Assistant at the University of Kentucky, Department of Mechanical Engineering, (January 2002 - December 2003)

Technical Publications

P. Singh, K. Kuwana, M. Hassan, and K. Saito, "Scale Model Experiments and Numerical Study on a Steel Teeming Process", *Fourth International Symposium for Scale Modeling, Cleveland, Ohio, Sept 17-19, 2003*